Spring 2014

Conceptual design using multilevel continuum structural topology optimization

Bodi Lu
University of Iowa

CONCEPTUAL DESIGN USING MULTILEVEL CONTINUUM STRUCTURAL TOPOLOGY OPTIMIZATION

by

Bodi Lu

A thesis submitted in partial fulfillment
of the requirements for the Master of Science degree
in Civil and Environmental Engineering
in the Graduate College of
The University of Iowa

May 2014

Thesis Supervisor: Professor Colby C. Swan

Graduate College
The University of Iowa
Iowa City, Iowa

CERTIFICATE OF APPROVAL

_____

MASTER'S THESIS

_____

This is to certify that the Master's thesis of

Bodi Lu

has been approved by the Examining Committee
for the thesis requirement for the Master of Science
degree in Civil and Environmental Engineering
at the May 2014 graduation.

Thesis Committee: _____
Colby C. Swan, Thesis Supervisor

_____
Jasbir S. Arora

_____
Salam Rahmatalla

ACKNOWLEDGMENTS

I would like to express my deep gratitude to my advisor, Professor Colby C. Swan for all of his patient guidance, valuable advice, and enthusiastic encouragement, and belief throughout my research work at The University of Iowa. His willingness to motivate me contributed tremendously to my research. The knowledge I have gained from Professor Swan is invaluable.

I would also like to thank Professor Jasbir S. Arora, Professor M. Asghar Bhatti and Professor Salam Rahmatalla for their great teaching in courses I took.

My special thanks to PhD students Yuanming Luo for his recommendations on my research and assistance with my studies.

Finally, I wish to thank my parents for their support and encouragement throughout my study.

TABLE OF CONTENTS

LIST OF TABLES

LIST OF FIGURES

CHAPTER 1

INTRODUCTION

1.1 A review of topology optimization

Topology optimization is a relatively new and speedily developing field of structural mechanics. It has become a powerful tool in computer-aided engineering, for the reason that it helps designers to gain insight into alternative topological possibilities other than size and shape. In the past three decades, considerable efforts have been made toward the development of this field. Although the basic principles of topology optimization have been known for centuries, the first systematic contribution to this field is regarded as the study of Michell (1904) in which an optimization resulting in thin-bar trusses with regard to weight was developed. Much later Prager and Rozvany (1976) solved a range of different topology optimization problems by analytical procedures based on optimality criteria.

Two types of structure exist in structural topology optimization: discrete structures and continuum structures. The research on discrete structural topology optimization has been active for several decades and largely developed by Prager and Rozvany (1976). Since the implementation of discrete structural topology optimization is ongoing but not yet practicable, people commonly adopt continuous optimization strategies by which an optimization problem is solved over a set of finite elements obtained from meshing of the continuum structural domain. This research has been extremely active since the publication of the paper by Bendsøe and Kikuchi (1988). In continuum structural topology optimization (CSTO), the shape of structural boundaries and the number of inner holes are optimized simultaneously with respect to one or more design objectives and constraints.

In continuum structural topology optimization, one deals with a cloud of porous structural material distributed throughout the structural domain. Where the porosity

vanishes the material is solid, and where it tends to unity the material is void. To compute the effective properties for porous solid-void materials, homogenization theory was originally employed by Bendsøe and Kikuchi (1988) by treating the porous material as having periodic microstructures. Their homogenization approach to continuum structural topology optimization yielded a mathematically well-founded theory, where they simulated holes by allowing the stiffness of the composite tend to zero (Stainko, 2006). Nevertheless, a year later Bendsøe (1989) offered a different and simplified approach that deals with isotropic porous materials using approximate power laws to represent their stiffness as a function of the solid volume fraction. This microstructure-free approach is now called the SIMP method (Solid Isotropic Material with Penalization), and is widely adopted in the field.

Sizing, shape and topology optimization problems address different aspects of the structural design problem (Bendsøe, 2003). Typically in a size optimization problem or a shape optimization problem, the aim is to find the optimal thickness or the optimum shape of a domain or member cross-section. In topology optimization the goal also includes finding optimal features such as the number and location and shape of holes, and the connectivity of the structural material domain. It is the most general area of structural optimization since it can determine where and where not to put material in a design space. Topology is a mathematical field which concerns the properties of geometric configurations that are unaltered by homeomorphic deformation or mappings (Swan, 2013). An example of a homeomorphic mapping is shown in the Figure 1.1 at the left hand side; where the original and new object may have a different shape but the topology is same. For the non-homeomorphic transformation at the right hand side, the connectivity of the new object is altered by the newly generated holes which means that the topology of two objects is different. Two spaces are homeomorphic if one can be deformed into the other without cutting or gluing. In Hubbard's book (1995) he mentioned that there is an old joke in mathematics field that goes "a topologist cannot tell

the difference between a coffee mug and a doughnut". This sentence can be interpreted by assuming both donut and mug as pliable and can be sufficiently reshaped. Thus the transformation can easily be complete by reshaping one side of the donut into a dimple and remaining the other side of the donut unaltered which can be treated as the handle of the mug. During the transformation, the connectivity remains the same and each space is of only one hole. Figure 1.2 shows this homeomorphic transformation from a coffee mug to donut, while Figure 1.3 shows examples of size, shape and topology variations in mechanical systems.

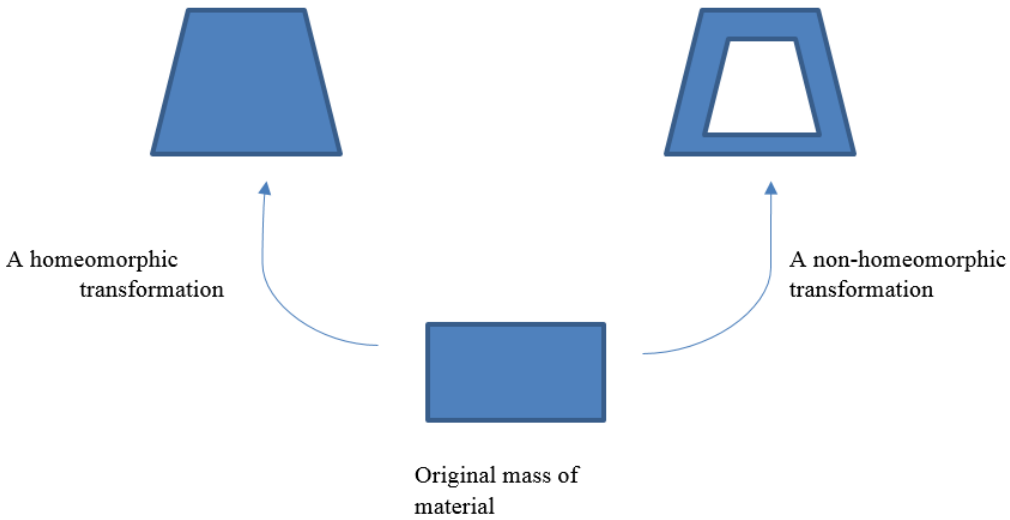

Figure 1. 1: Homeomorphic and non-homeomorphic transformation.

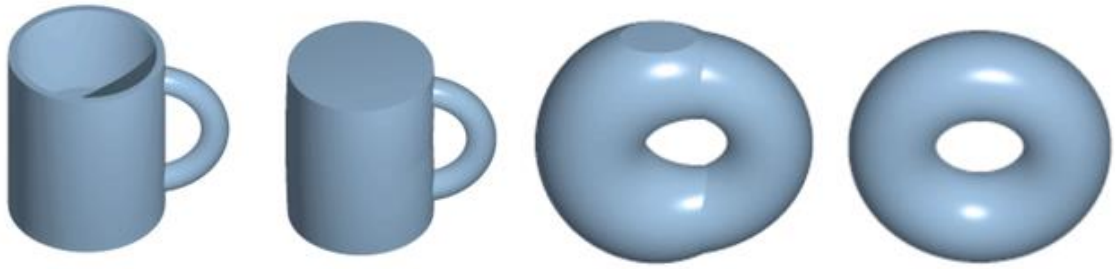

Figure 1. 2: An example of homeomorphic transformation (LucasVB, 2006).

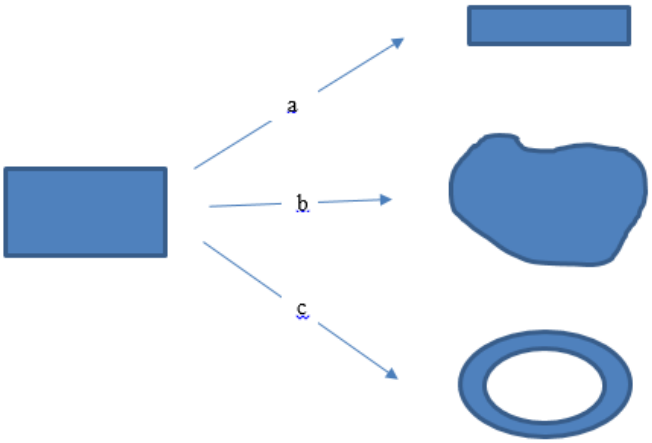

Figure 1. 3: Examples of mechanical system changes. (a) Size change where only a single dimension is varied. (b) Shape changes where the exterior boundary of the domain varies; and (c) Size, shape and topology changes.

1.2 Usage of CSTO in engineering disciplines

Continuum structural topology optimization is today being successfully applied in a diverse array of engineering fields: automobile, aeronautical, micro-systems, structural and industrial. Since this method has been found to be very efficient for material layout optimization at the preliminary design stage, it has been applied for a number of performance objectives, such as: minimal compliance, tuned natural frequency period, maximized critical buckling load, tuned material properties in composites, and performance of continuous micro-mechanisms. By applying boundary conditions, such as sets of load and the degree of freedom, and adding constraint such as material occupancy, structural features that optimize the designed structural performance can be obtained (Figure 1.4)

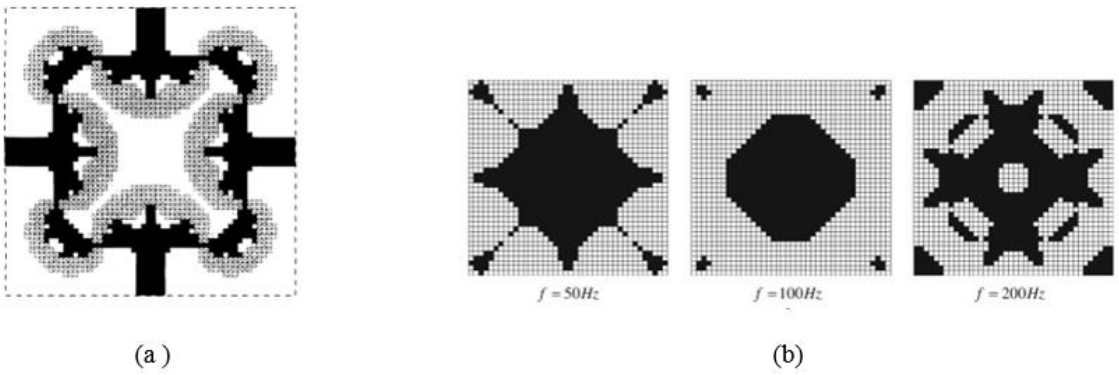

Figure 1. 4: Two examples of the topology optimization application in applied mechanics. (a) Optimal microstructure for minimization of effective thermal strain coefficient studied by Sigmund (1998). (b) Optimal material layouts in a plate with respect to sound radiation at three significantly different frequencies (Xu, 2011).

CSTO is even being used in structural engineering practice by some of today's leading structural engineering firms. To illustrate, Figure 1.5 shows an example, in which part of a complex structure was optimized with CSTO. With the load case and boundary conditions shown in (a), the topology optimization resulting design has more bracing members around the supports. Figures 1.5 (c) and Figure 1.6 show how a resulting design can be interpreted and achieved in built structures.

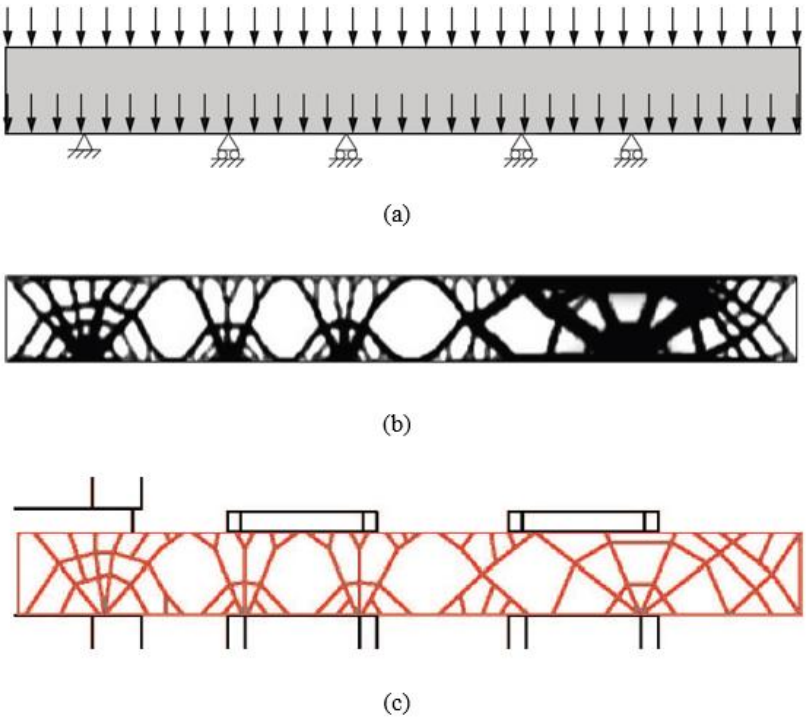

Figure 1. 5: Example of topology optimization application in structure (Beghini, 2013). (a) Structural domain with loading and support conditions. (b) material layout distribution for minimal compliance under the load case shown; (c) Resulting engineering interpretation.

Figure 1. 6: Implementation of structural topology optimization results in architectural rendering by Skidmore, Owings & Merrill (SOM). (Beghini, 2013).

1.3 Commercial availability

Continuum structural topology optimization is now available in a number of commercial finite element analysis codes, such as Abaqus/ATOM, Ansys, Genesis, NX Topology optimization, Optistruct, and TOSCA, which provide convenience for engineers doing computer aided design.

To illustrate the general point about CSTO availability in commercial analysis codes, we consider the specific example of the Abaqus Topology Optimization Module (ATOM). It is able to solve a vast amount different material layout optimization problems, including those of structural, thermal, flow, electrical and magnetic natures. In general, there are three different approaches to optimizing a structure using Abaqus ATOM:

1) Minimize strain energy, constrained with an upper bound on the relative volume fraction.

2) Minimize the volume, constrained with an upper bound for displacement, moment of inertia, reaction forces, or rotation.

3) Maximize Eigen-frequencies, constrained with a lower limit for volume or limits for other design responses that are independent of loads (as eigenvalue analysis are performed without external forces applied) (Johnsen, 2013).

In the design results, Abaqus ATOM provides not only the material layout of the structure, but also the contours for structural displacements and stress, and cost function graphs with respect to many structural properties (Figure 1.7).

Figure 1. 7: Optimal result of a structure solved by Abaqus ATOM (Johnsen, 2013).

1.4 Thesis Objectives

A multilevel approach to CSTO is investigated in this thesis. This basic idea of the multilevel approach is to begin solving CSTO problems on relatively coarse meshes and to then continue the design process on a sequence of increasingly refined meshes. The multilevel approach provides the possibility of significant computational saving when applied together with analysis problem reduction techniques that intelligently excludes broad swaths of continuous void domains from the analysis problems. In the doctoral dissertation of Stainko (2006), a minimal compliance problem was treated in the framework of an adaptive multilevel approach with the computational time recorded. In addition, a fuzzy tolerance multilevel optimization approach was proposed in a study by Luo et al (2006) to overcome the drawbacks of traditional programming schemes. However not many researches have a time record of the optimization process, and no one

has reported research focused on the analysis time comparison between single level and multilevel problems.

In this study, the multilevel approach is investigated in the context of optimizing a canyon bridge frame. To provide realistic design solutions for structures such as long-span bridges, continuum topology optimization must deal with sparse structures on large, finely meshed domains which result in very high computational intensity. To alleviate this problem both a multi-level refinement method and an analysis problem size reduction technique are applied in the optimization process. The efficiency of the multilevel approach is studied by using analysis time as a judgment criterion. To make sure that design solutions obtained with the proposed methods are both constructible and convergent with mesh refinement, a perimeter control method is employed in this framework. A result of this study is analysis made on both structural layout and objective function history with respect to iteration counts.

CHAPTER 2

METHODS

2.1 Optimization procedure

The optimization problem proceeds with the following steps:

Step 1: At the outset of the optimization, a set of initial values are assigned to design variables. In a general optimization problem all values are set to 1 or 0 which means the whole design domain is solid or void at the very beginning. In a multilevel problem, the initial values are from the results of a lower level mesh.

Step 2&3: Then with the initial values, finite element analysis is made. Evaluation of displacements and stress are made during this analysis. Calculation of constraint functions and objective functions is carried out.

Step 4: The sensitivities of the constraints and the objective function to changes in the design variables are computed.

Step 5: If the convergence criteria for the optimization algorithm are satisfied, then the optimum solution has been found and the solution process is terminated. If not, the optimization would go to the next step.

Step 6: A mathematical programming method, sequential linear programming SLP algorithms, is used to update the design variables. The problem goes back to step 2, and a new round of iteration starts.

The whole procedure is depicted in Figure 2.1.

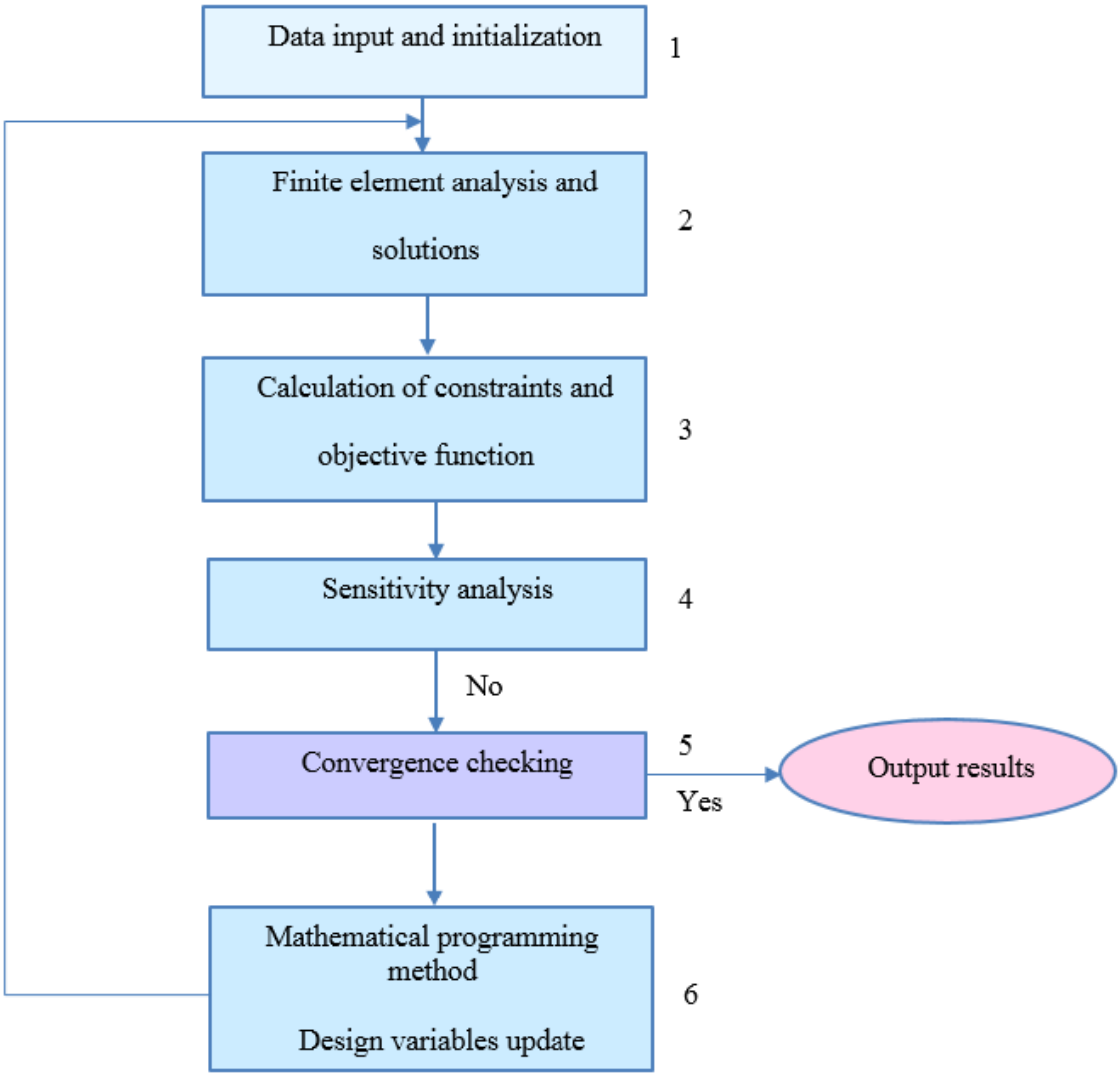

Figure 2. 1: Flowchart of the topology optimization procedure.

2.2 Formulation

When a structure features a linear elastic response behavior, the expression between the applied external loads $\mathbf{f}^{ext}$ and the resulting displacement field $\mathbf{u}$ can be written as:

$$\mathbf{r} = \mathbf{0} = \mathbf{K}\mathbf{u} - \mathbf{f}^{ext} \tag{2.1}$$

where $\mathbf{K}$ represents the stiffness matrix of the structure. In this study, the single-objective is minimizing the compliance of the structure subject to an upper bound C on the volume of solid material in the structure ($C \in [0,1]$). Compliance M measures the external work done on the structure. It is the sum of all the displacements at the points where the load is applied, weighted by the magnitude of the loading. Thus by using this objective, the problem minimizes the defection of the structure due to applied loads. In other words it maximizes the stiffness of the structure under a specific loading case, $\mathbf{f}^{ext}$.

$$\mathrm{M}(\mathbf{u},\mathbf{b}) = \frac{1}{2}\mathbf{f}^{ext} \cdot \mathbf{u} \tag{2.2}$$

Structural concept designs are encoded in the design vector $\mathbf{b}$ which is a vector of continuous nodal variables, each on the $[0,\ 1]$ interval. Each nodal design variable represents the solid volume fraction at a node in the structural model. The stiffer the structural concept designs $\mathbf{b}$, the smaller the objective function values M will be.

The generalized formulations for a minimum compliance problem involving both force and displacement loadings of a structure can be expressed as (Swan,2013):

$$\min_{b}[\mathrm{M}(\mathbf{u},\mathbf{b}) = \frac{1}{2}(\mathbf{f}^{ext} \cdot \mathbf{u} - \sum_{E \in \eta_g} \mathbf{f}_{\mathrm{E}}^{\mathrm{int}} \cdot \mathbf{g}_E)] \tag{2.3}$$

Such that

$$\mathrm{r}(\mathbf{u},\mathbf{b}) = \mathbf{0} \tag{2.4}$$

$$\phi(\boldsymbol{X}) = \sum_{\mathrm{A}} \mathrm{N}_{\mathrm{A}}(\mathbf{X})\phi_A \tag{2.5}$$

$$\frac{1}{V}\int \phi \, d\Omega - C \le 0 \tag{2.6}$$

$$b_l \le b_i \le b_u \tag{2.7}$$

Above, $0 = b_l$ and $1 = b_u$ are the lower and upper bound of each design variable b_{i} ; $\mathbf{f}_E^{int}$ represents an internal force at a node E where a displacement loading $\mathbf{g}_E$ is applied; $\mathbf{r}$ denotes the residual of the force-balance structural equilibrium. Since the structure is in a state of minimum potential energy, the equality constraint is $\mathbf{r} = \mathbf{0}$; ϕ denotes the solid volume fraction field in the structural domain.

2.3 Boundary value problems

2.3.1 Static admissibility conditions

In a standard elastostatic boundary value problem in solid mechanics, each point in the structural domain Ω satisfies the local equilibrium condition:

$$\sigma_{\mathrm{ij,i}} + \rho\, \gamma_{\mathrm{j}} = 0 \tag{2.8}$$

Here σ_{ij} is the local Cauchy stress, ρ is the local mass density, and γ_{j} represents a vector of body force. There are two different regions for the boundary of Ω . One is the

boundary Γ_h where surface traction $\mathbf{h}$ applied , and the other is the boundary Γ_g where prescribed displacements $\mathbf{g}$ are applied. From equation (2.8), we have,

$$\int_{\Omega} \left(\sigma_{ij,i} + \rho \gamma_j \right) \delta u_j \, d\Omega = 0 \tag{2.9}$$

where u_j denotes the continuous variational displacement field. From vector calculus, and integration by parts, the first term in equation (2.9) can be expressed as:

$$\int_{\Omega} \sigma_{ij,i} \delta u_j \, d\Omega = \int_{\Gamma} h_j \delta u_j \, d\Gamma - \int_{\Omega} \sigma_{ij} \delta \varepsilon_{ij} d\Omega = 0 \tag{2.10}$$

Substituting of equation (2.10) into equation (2.9), leads to the following expression which equates internal virtual work to external virtual work.

$$\int_{\Omega} \sigma_{ij} \delta \varepsilon_{ij} d\Omega = \int_{\Gamma} h_i \delta u_j d\Gamma + \int_{\Omega} \rho \, \gamma_j \delta u_j d\Omega \tag{2.11}$$

$$\delta W_{int} = \delta W_{ext}$$

2.3.2 Potential energy

The infinitesimal elastic strains related to displacements can be expressed as:

$$\varepsilon_{ij} = \frac{1}{2} \left(u_{i,j} + u_{j,i} \right) \tag{2.12}$$

When the material obeys a linear elastic constitutive law, the resulting stress is:

$$\sigma_{ij} = E_{ijkl}\varepsilon_{kl} \tag{2.13}$$

The strain energy density R at a point in the structural domain is:

$$\mathrm{R} = \frac{1}{2}\boldsymbol{\sigma} : \boldsymbol{\varepsilon} \tag{2.14}$$

If R is the quadratic strain energy function for a linear elastic solid, it can be expressed as:

$$\mathrm{R} = \frac{1}{2}\varepsilon_{ij}E_{ijkl}\varepsilon_{kl} \tag{2.15}$$

Taking the derivative of R with respect to $\boldsymbol{\varepsilon}$, yields the stress which is the gradient of the strain energy.

$$\sigma_{ij} = \frac{\partial \mathrm{R}}{\partial \varepsilon_{ij}} = E_{ijkl}\varepsilon_{kl} \tag{2.16}$$

The differential of elastic strain energy can be written as:

$$\delta \mathrm{R} = \sigma_{ij}\delta\varepsilon_{ij} = \frac{\partial \mathrm{R}}{\partial \varepsilon_{ij}}\delta\varepsilon_{ij} \tag{2.17}$$

It follows that the internal virtual work in a system is the variation of the elastic strain energy:

$$\delta \mathrm{W}^{\mathrm{int}} = \int_{\Omega} \sigma_{ij}\delta\varepsilon_{ij}\, d\Omega = \int_{\Omega} \delta \mathrm{R}\, d\Omega \tag{2.18}$$

Now taking a close look at the external virtual work, the term $\rho\gamma_j\delta u_j$ denotes the body forces work contribution

$$\delta\Phi = -\rho\boldsymbol{\gamma}\cdot\delta\mathbf{u} \tag{2.19}$$

$$\Phi = -\rho\gamma\cdot\mathbf{u} \tag{2.20}$$

In a similar manner, $h_i\delta u_j$ denotes the contribution of traction forces to external virtual work.

$$\delta\psi = -\mathbf{h}\cdot\delta\mathbf{u} \tag{2.21}$$

$$\psi = -\mathbf{h}\cdot\mathbf{u} \tag{2.22}$$

Putting these two together, external virtual work can be expressed as:

$$\delta W^{ext} = -\left(\int_\Gamma \delta\psi d\Gamma + \int_\Omega \delta\Phi d\Omega\right) \tag{2.23}$$

The potential energy Π of a body or system is the sum of the elastic strain energy and the force potentials, and can be expressed as:

$$\Pi = \int_\Omega R d\Omega + \int_\Gamma \psi d\Gamma + \int_\Omega \Phi d\Omega \tag{2.24}$$

$$\delta\Pi = \int_\Omega \delta R d\Omega + \int_\Gamma \delta\psi d\Gamma + \int_\Omega \delta\Phi d\Omega \tag{2.25}$$

$$\delta\Pi = \int_\Omega \sigma_{ij}\delta\varepsilon_{ij} d\Omega - \left(\int_\Gamma h_i\delta u_j d\Gamma + \int_\Omega \rho\gamma_j\delta u_j d\Omega\right) \tag{2.26}$$

If a system is stationary with regard to Π then $\delta\Pi = 0$ which corresponds to satisfaction of virtual work equation.

2.4 Design domain discretization

In a finite model, the structural domain Ω is discretized into a number of non-overlapping finite elements.

$$\Omega = \bigcup_{i=1}^{numel} \Omega_i \tag{2.27}$$

where $numel$ is the number of elements and Ω_i is the region of the i^{th} element in the model. The vertices of the elements are taken as the nodal points.

The displacement field $\mathbf{u^h}$ associated with the above discretization can be expressed by a finite dimensioned vector of unknowns:

$$\mathbf{u}^h(\mathbf{X}) = \sum_{i=1}^{numnp} N_i(\mathbf{X})\mathbf{d}_i \tag{2.28}$$

Here, $N_i(\mathbf{X})$ represents the shape or interpolation functions which in this particular study are C^0 continuous and the first derivatives are piecewise continuous; $\mathbf{d}$ is a displacement vector of dimension $numnp * ndof$ in which $numnp$ is the number of nodes and $ndof$ is the number of degrees of freedom for each node. The infinitesimal strain at a given point in the body can be written as:

$$\varepsilon_{ij}^h = \frac{1}{2}\left(u_{i,j}^h + u_{j,i}^h\right) \tag{2.29}$$

Commonly in the finite element analysis, for the sake of convenience the strain and stress are expressed in vectors rather than matrices.

$$\boldsymbol{\varepsilon}=\left[\varepsilon_{11},\varepsilon_{22},\varepsilon_{33},\gamma_{23},\gamma_{13},\gamma_{12}\right];\quad \boldsymbol{\sigma}=\left[\sigma_{11},\sigma_{22},\sigma_{33},\sigma_{23},\sigma_{13},\sigma_{12}\right].$$

At a given point in the body, the strain and the variational strain can be written as a summation:

$$\boldsymbol{\varepsilon}^{h}\left(\boldsymbol{X}\right)=\sum_{\mathrm{L}=1}^{numnp}\mathbf{B}_{\mathrm{L}}\left(\boldsymbol{X}\right)\mathbf{d}_{\mathrm{L}} \tag{2.30}$$

$$\delta\boldsymbol{\varepsilon}^{h}\left(\boldsymbol{X}\right)=\sum_{M\in\{\eta\setminus\eta_{\mathrm{g}}\}}\mathbf{B}_{M}\left(\boldsymbol{X}\right)\mathbf{c}_{M} \tag{2.31}$$

where $\mathbf{c}_{\mathrm{M}}$ is the variational displacement vector at unrestrained node M. $\mathbf{B}_{\mathrm{L}}\left(\boldsymbol{X}\right)$ denotes the strain displacement matrix associated with the L^{th} node and has the specific composition:

$$\mathbf{B}_{\mathrm{L}}=\begin{pmatrix}\mathrm{N}_{L,1} & 0 & 0\\ 0 & \mathrm{N}_{L,2} & 0\\ 0 & 0 & \mathrm{N}_{L,3}\\ 0 & \mathrm{N}_{L,3} & \mathrm{N}_{L,2}\\ \mathrm{N}_{L,3} & 0 & \mathrm{N}_{L,1}\\ \mathrm{N}_{L,2} & \mathrm{N}_{L,1} & 0\end{pmatrix} \tag{2.32}$$

Substituting equations (2.28) and (2.31) into equation (2.10), yields:

$$\sum_{M\in\{\eta/\eta_g\}}\left[\int_{\Omega}\boldsymbol{\sigma}\,\boldsymbol{B}_M\,\mathbf{c}_M\,d\Omega-\int_{\Gamma}\mathbf{h}\mathrm{N}_M\mathbf{c}_M\,d\Gamma-\int_{\Omega}\rho\boldsymbol{\gamma}\mathrm{N}_M\mathbf{c}_M\,d\Omega\right]=0 \tag{2.33}$$

Since this equality must be satisfied for all real and bounded values of $\mathbf{c}_{\mathrm{M}}$ it follows that

$$\int_{\Omega}\boldsymbol{B}_M^T\boldsymbol{\sigma}\,d\Omega=\int_{\Gamma}\mathbf{h}\mathrm{N}_{\mathrm{M}}d\Gamma+\int_{\Omega}\rho\boldsymbol{\gamma}\mathrm{N}_{\mathrm{M}}d\Omega \tag{2.34}$$

In equation (2.34) the left side is the internal force at the M^{th} node, and the right hand side is the external force on the same node.

$$(\mathbf{f}^{M})^{int}=(\mathbf{f}^{M})^{\mathrm{ext}} \tag{2.35}$$

$$\mathbf{r}^{M}=(\mathbf{f}^{M})^{int}-(\mathbf{f}^{M})^{\mathrm{ext}}=\mathbf{0} \tag{2.36}$$

Equation (2.36) expresses a force equilibrium at the M^{th} unrestrained node at the model. This equation can also be written more globally, for all nodes, as:

$$\mathbf{r}=\mathbf{f}^{int}-\mathbf{f}^{ext}=\mathbf{0} \tag{2.37}$$

where $\mathbf{r}$ is the global equilibrium residual of the structure.

In computational models, the stress and strain can be expressed in a condensed vector form as noted. It follows that the elasticity tensor will take the form of a symmetric 6×6 matrix. Thus, equation (2.13): $\sigma_{\mathrm{ij}}=E_{\mathrm{ijkl}}\varepsilon_{\mathrm{kl}}$ can be condensed to

$$\sigma_{\mathrm{i}}=E_{ij}\varepsilon_{\mathrm{j}} \tag{2.38}$$

When substituted into equation (2.34),

$$\text{for } M \in \left\{\eta \setminus \eta_{\mathrm{g}}\right\} \qquad \int_{\Omega} \mathbf{B}_M^T \mathbf{E} \mathbf{B} d\Omega \cdot \mathbf{d} = \int_{\Gamma} \mathrm{N} \mathbf{h} d\Gamma + \int_{\Omega} \mathrm{N} \rho \gamma d\Omega \tag{2.39}$$

Furthermore,

$$\mathbf{B} \cdot \mathbf{d} = \sum_{L \in \left\{\eta \setminus \eta_{\mathrm{g}}\right\}} \mathbf{B}_L \cdot \mathbf{d}_L + \sum_{E \in \eta_{\mathrm{g}}} \mathbf{B}_E \cdot \mathbf{g}_E \tag{2.40}$$

2.5 Interpolation of design variables

There are a number of interpolation function spaces for design variables and displacements fields to choose from when implementing continuum structural topology optimization formulations. Q4/U is a popular implementation with nodal displacements interpolated using the bilinear quadrilateral element shape functions, and the design variables piecewise uniform on the element domains. However, for the design variable fields this implementation does not ensure C^0 continuity, and for compliance minimization problems with the Q4/U implementation, checkerboard layout patterns frequently occur for the reason that the solid and void material design turns out to be artificially stiff (Diaz and Sigmund 1995). An older but effective method to eliminate checker boarding with Q4/U formulation is the spatial filtering (Sigmund O, Petersson J 1998; Swan and Kosaka 1997) of design variables together with penalized mixing rules. The spatial filtering renders checker boarding regions into grey mixtures which are very compliant with penalized mixing rules. With checkerboard solutions no longer featuring artificially high stiffness, they are no longer obtained by the optimizer seeking low compliance solutions.

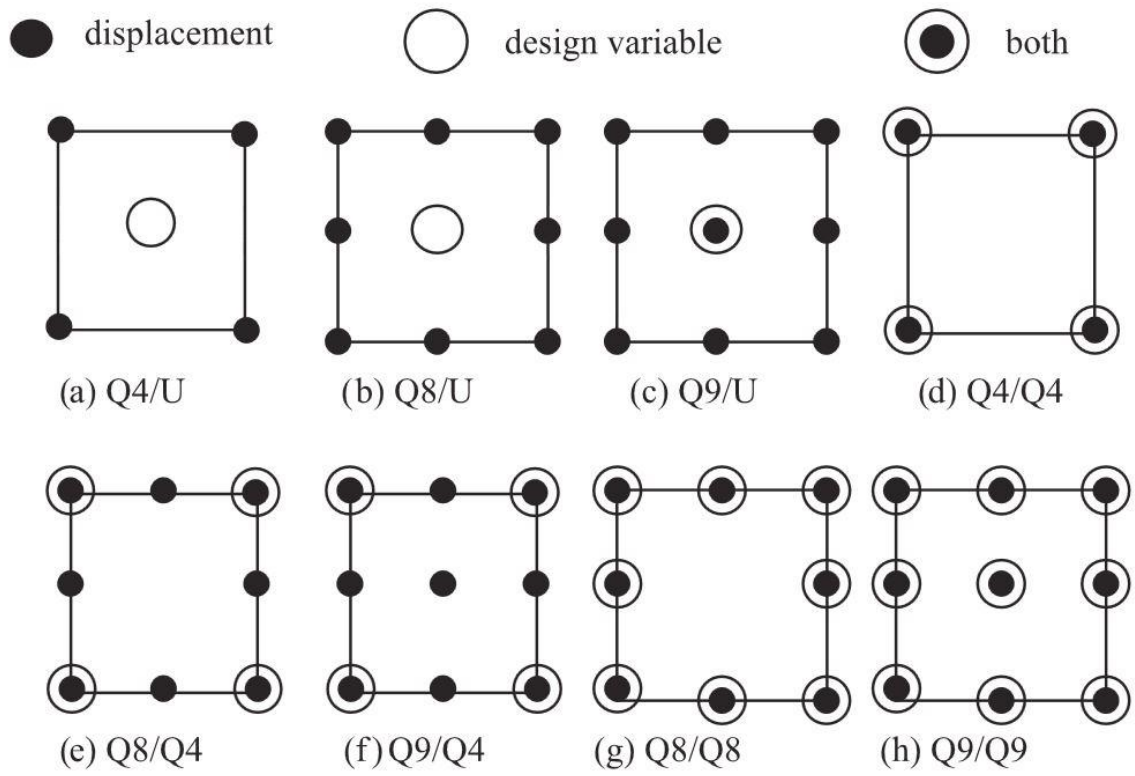

Figure 2. 2: Eight possibilities for two-dimensional element-wised interpolation of displacement fields and design variable fields (Rahmatalla and Swan 2004)

New interpolation combinations have been explored in more recent studies, such as the Q4/Q4M implementation (modified Q4/Q4 implementation) (Paulino, Le 2008). This approach uses a regular Q4 element for the displacement field and four nodes located at midpoints of the element edges to interpret the design variable field. Together with the CAMD approach (Matsui and Terada, 2004) and internal averaging technique,

the Q4/Q4M implementation has been shown to provide a high resolution without increasing mesh refinement and also final designs without any apparent numerical instabilities.

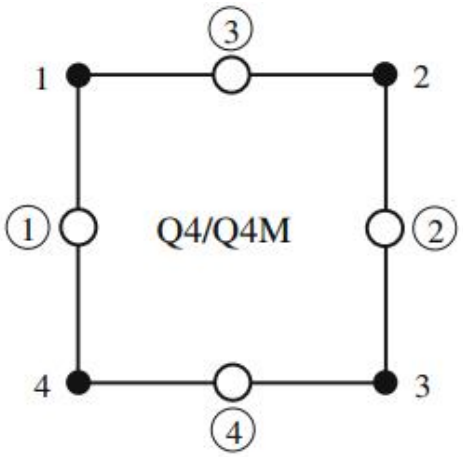

Figure 2. 3: Q4/Q4M element-wise interpolation of displacements and design variables (Paulino, Le 2008)

In this study, the Q4/Q4 implementation is used, with both displacements and design variables being associated with the same nodes and the same nodal interpolation functions. Accordingly, the solid volume fraction field within the model domain takes the following form:

$$\phi(\boldsymbol{X}) = \sum_{A=1}^{nump} \mathrm{N_A}(\mathbf{X})\phi_A \tag{2.41}$$

Where $\mathrm{N_A}$ is the A^{th} nodal interpolation function and ϕ_A denotes the solid nodal volume fraction of at node A. Physically, $\phi(\boldsymbol{X})$ is the fraction of an infinitesimal volume surrounding point $\boldsymbol{X}$ occupied by solid material.

Although Q4/Q4 design formulation is able to ensure C^0 continuity of design variables, it can still yield designs with numerical instabilities. This problem is well represented in the MBB beam problem (Rahmatalla and Swan 2004). In Figure 2.4, the material layout shows apparently "layering" and "islanding" of black and white regions inside the beam, which would be difficult to interpret from a design perspective and also have a bad effect on the convergence of the design solutions. Perimeter constraints are utilized in this work to help alleviate these problems.

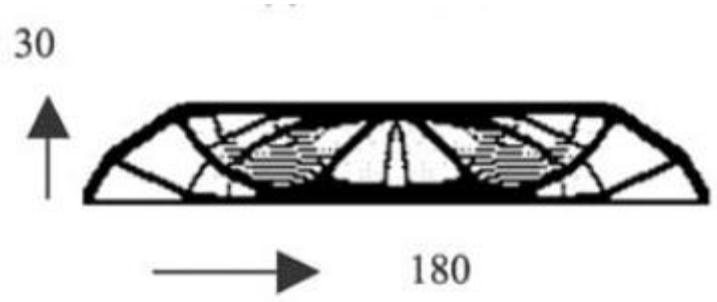

Figure 2. 4: A MBB beam problem designs achieved with the Q4/Q4 formulation that features "layering" and "islanding" (Rahmatalla and Swan 2004)

2.6 Mixing Rule

Generally in a design domain Ω, each single element contains a mixture of two materials, and so a constitutive relationship between strain and stress for this mixture is needed. It is assumed in this study that both the solid material A and the void material B feature linear elastic material behaviors.

$$\boldsymbol{\sigma}_A = \mathbf{E}^A \cdot \boldsymbol{\varepsilon}_A ; \quad \boldsymbol{\sigma}_B = \mathbf{E}^B \cdot \boldsymbol{\varepsilon}_B \tag{2.42}$$

Several methods can be used obtain effective elastic properties $\mathbf{E}$ for a mixture element relating the effective stress $\boldsymbol{\sigma} = \phi_A \boldsymbol{\sigma}_A + \phi_B \boldsymbol{\sigma}_B$ to the effective strain $\boldsymbol{\varepsilon} = \phi_A \boldsymbol{\varepsilon}_A + \phi_B \boldsymbol{\varepsilon}_B$. The Voigt (isostrain) rule of mixtures assumes that $\boldsymbol{\varepsilon}_A = \boldsymbol{\varepsilon}_B$ and yields that:

$$(\mathbf{E}^*)^{Voigt} = \phi_A \mathbf{E}^A + \phi_B \mathbf{E}^B \tag{2.43}$$

Alternatively, the isostress Reuss rule of mixtures assumes that $\boldsymbol{\sigma}_A = \boldsymbol{\sigma}_B$ and yields that:

$$(\mathbf{E}^*)^{Reuss} = [\phi_A (\mathbf{E}^A)^{-1} + \phi_B (\mathbf{E}^B)^{-1}]^{-1} \tag{2.44}$$

Usually the Reuss rule is used for the case that the moduli of two materials are fairly close to each other. Otherwise, this rule would experience a discontinuity at $\phi_A = 1$ when $\|\mathbf{E}^A\| \gg \|\mathbf{E}^B\|$. To address this problem, a hybrid Voigt-Reuss mixing rules is used:

$$(\mathbf{E}^*)^{hybrid} = \alpha (\mathbf{E}^*)^{Voigt} + (1-\alpha)(\mathbf{E}^*)^{Reuss} \tag{2.45}$$

with hybridizing parameter $\alpha \in [0,1]$.

In this study, the power law mixing rule which is also called SIMP method (Solid Isotropic Material with Penalization) is used. The effective stiffness for this method is:

$$\mathbf{E}^{*} = \phi_A{}^{p}\mathbf{E}^{A} + \left(1-\phi_A{}^{p}\right)\mathbf{E}^{B} \tag{2.46}$$

where the mixing rule parameter $p \in [1,4]$. When $p=1$, SIMP recovers the Voigt mixing rule which does not penalize the mixtures. In this case, it yields a convex compliance functional so that there is only one solution for the problem. However, the design result may seem very "grey". And thus be difficult to interpret . With $p=4$, the optimization problem is generally not convex and the objective function value, and several local solutions could exist, though the design result seems very "black and white" which means that the region would be either solid or void. In this study, the power law mixing rule is typically used with a parameter $p=2.5$ in all computations.

2.7 Mathematical programming method

During the optimization process, mathematical programming is employed to minimize the objective function while satisfying the constraints. There are several choices for the mathematical programming method, such as Sequential Linear Programming (SLP), Sequential Quadratic Programming (SQP), and the Method of Moving Asymptotes (MMA). Sequential linear programming algorithms (SLP), have been employed successfully in numerous prior applications of CSTO and are thus used in this study. SLP is efficient for solving large nonlinear problems since it does not require second derivative information, and is the simplest convex approximation approach for a structural optimization problem with many simple constraints. This method consists of sequentially solving a series of linear sub-problems obtained by writing linear Taylor series expansions for the objective and constraint functions (Arora, 2012).

The sequential linear programming algorithm used in this study can be stated as follows (Mijar, 1997):

Step 1: Set iteration number to $k = 0$. Initialize a starting design $\mathbf{b}^{(0)}$ to $\mathbf{b}^{(k)}$ and select proper move limits Δ_M and stopping criteria parameters ε_1 and ε_2 .

Step 2: Evaluate both the objective $F^{(k)}(\mathbf{b})$ and inequality constraint functions $G^{(k)}(\mathbf{b})$ and their gradients $\nabla F^{(k)}(\mathbf{b})$ and $\nabla G^{(k)}(\mathbf{b})$ at k^{th} iteration.

Step 3: Solve the LP subproblem for $\mathbf{d}^{(k)}$.

$$\begin{aligned} &\text{Minimize} && \bar{f} = \nabla F^{(k)} \cdot \mathbf{d} \\ &\text{Subject to} && \nabla \mathbf{G}^{(k)} \cdot \mathbf{d} \le -\mathbf{G}^{(k)} \\ & && -\Delta_M \le \mathbf{d} \le \Delta_M \end{aligned} \tag{2.47}$$

where $\bar{f}$ is the linearized change in the original cost function; $\mathbf{d}$ is the vector for search direction.

Step 3: Use line search to find step size α_k such that $\Delta\mathbf{b}^{(k)} = \alpha_k \mathbf{d}^{(k)}$, and check the decent condition: $\nabla F \cdot \Delta\mathbf{b} < 0$. $\Delta\mathbf{b}$ denotes the design change. α_k represents step size and $\mathbf{d}^{(k)}$ is the search direction at the k^{th} iteration.

Step 4: Check for the convergence.

$$\left\| V^{(k)} \right\| \le \varepsilon_1 \tag{2.48}$$

$$\left\| \Delta\mathbf{b} \right\| \le \varepsilon_2 \tag{2.49}$$

where $V^{(k)}$ is the maximum constraint violation. If convergence, problem stops.

Step 5: Update the design vector $\mathbf{b}^{(k+1)} = \mathbf{b}^{(k)} + \Delta\mathbf{b}^{(k)}$ and update iteration counter $k = k + 1$. Return to step 2.

2.8 Numerical instabilities and perimeter constraint

Although the development of topology optimization has been significant in recent years, there still exist quite a few problems such as numerical instabilities that must be

handled carefully. Numerical instabilities, including checkerboards, mesh-dependence, and local minima, frequently appear in applications of CSTO. Local minima refers to the problem of obtaining different solutions when using different algorithmic parameters. In a stiffness topology optimization, checkerboarding happens when the process results in a checkerboard-like arrangement of material which is region with alternating solid and void elements (Figure 2.5). This arrangement can make the structure perform of a high artificial stiffness, but it makes shape extraction of structures difficult and the optimal structure hard to manufacture as well.

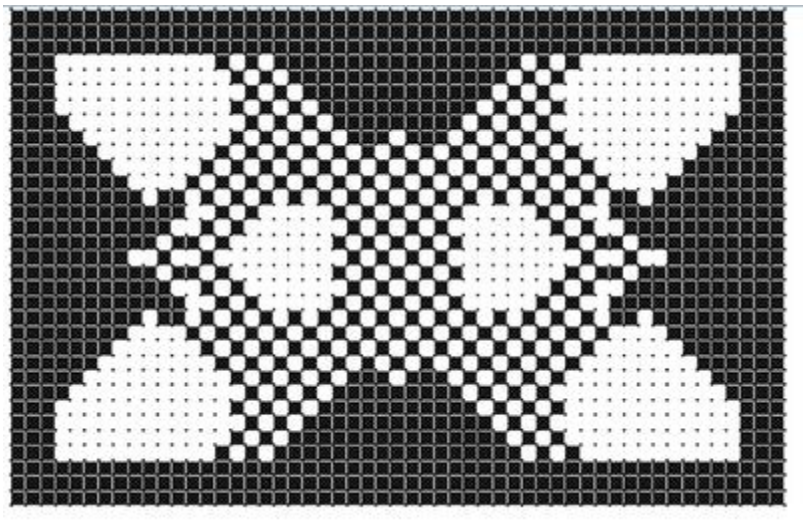

Figure 2. 5: Example of checkerboard problem (Li et al, 2000).

Mesh-dependency is another numerical instability in topology optimization, and it occurs when the continuum topology solution obtained does not converge with mesh refinement. Typically with mesh dependency as the mesh is refined, designs with increasingly intricate details and thus increasing perimeter occur. To illustrate the concept of perimeter, consider Figure 2.6 in which a single element is refined into four elements with a perimeter increasing from 8b to 16b.

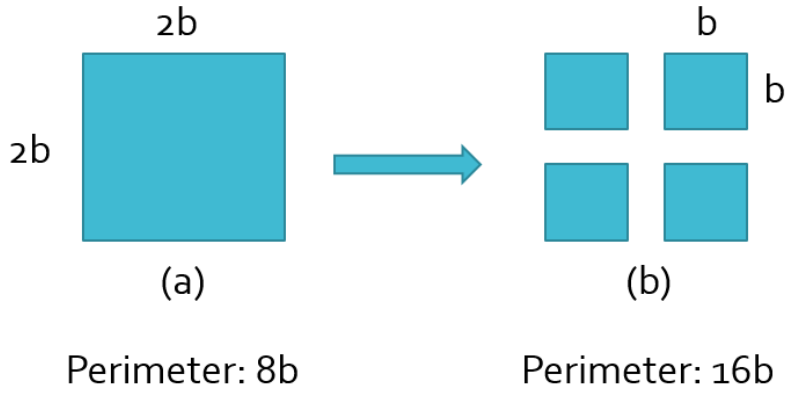

Figure 2. 6: Illustration of perimeter increasing: single element mesh refinement.

The perimeter constraint method, introduced by Haber et al (1996), is one of the most effective techniques to make refined continuum topology designs converge and to

alleviate checkerboard patterns as well. When refining a two dimension model into a finer mesh within a given volume, one unit with material may be divided into several small units and this would lead to a significant increasing of the total perimeter(or surface area in a three dimension model) and unwanted sub-units. By setting a bound to the entire perimeter of the solid material, this method can effectively restrict the fineness of the design. By introducing a sufficiently tight perimeter constraint into the problem, many sub-units would be eliminated.

The mesh-dependency problem and perimeter constraint method are well shown in the study of Rahmatalla and Swan in Figure 2.7 which is the MBB beam compliance minimization problem solved with a material usage constraint 50% that of the envelope structural volume. A simply supported structural domain with a central point load applied has a length to height ratio of 6:1, shown in Figure 2.7 (a). Using the Q4/Q4 implementation, the compliance minimization problem is solved with finite element model for the beam progressively refined. The resulting layout solutions shown in Figure 2.7 (b) – (d) displays increasing complexity with mesh refinement. These refined meshes feature non-convergent grillage type design solutions. When the problem is solved with a perimeter constraint enforced, the designs are free of the mesh-dependency problem. Figure 2.7 (e)-(f) shows three resulting layouts with different level of meshes that are essentially identical.

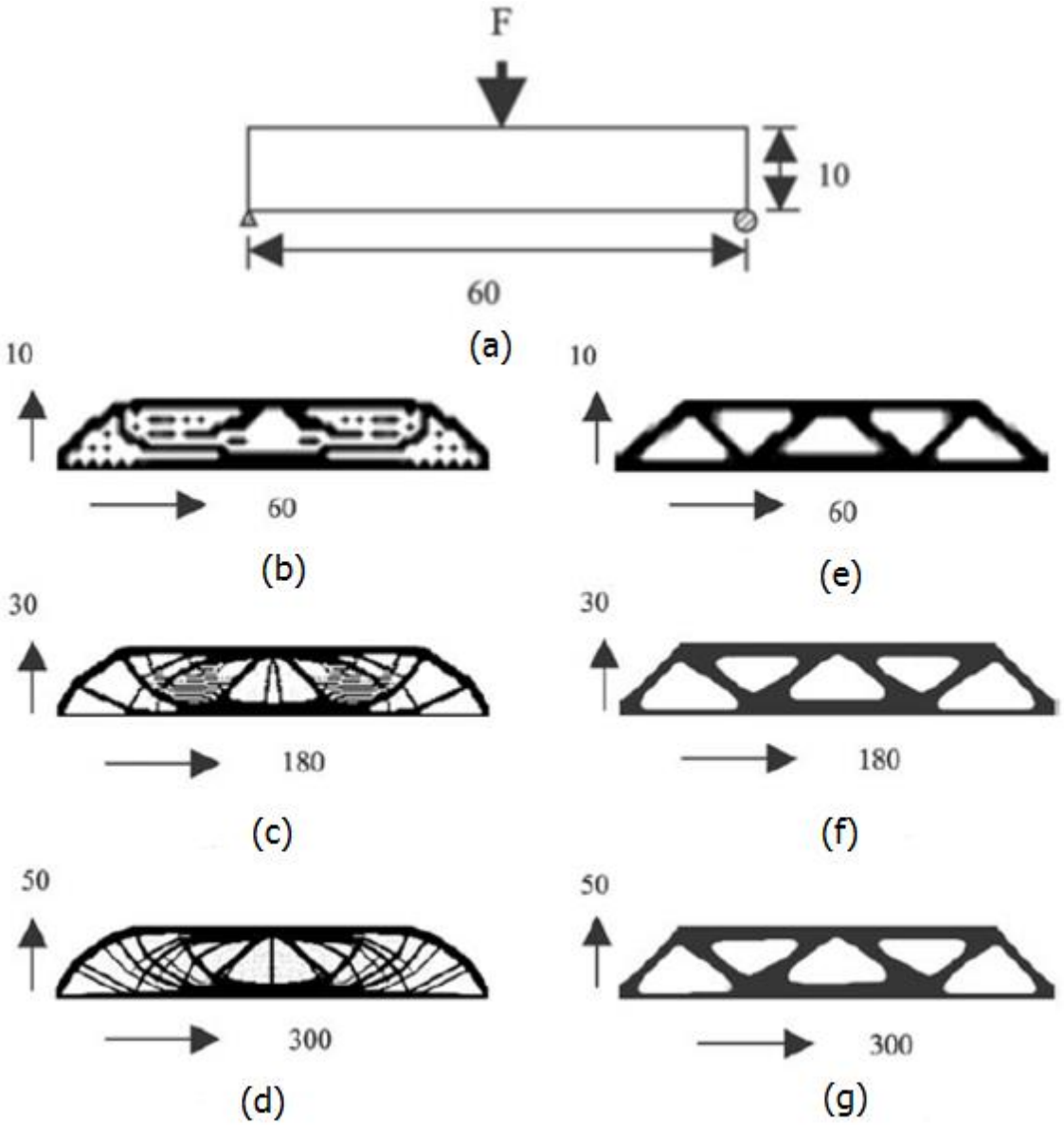

Figure 2. 7: The example of MBB beam design convergence with mesh refinement (Rahmatalla, 2004). Designs (b), (c) and (d) show lack of convergence as computational mesh is refined with or without perimeter constraint. When perimeter constraints are imposed, the design solutions (e), (f), and (g) are clearly convergent with mesh refinement.

CHAPTER 3

MULTILEVEL ALGORITHM

The continuum structural topology optimization process requires effort to determine where to take out material and where to place material, especially in very fine mesh problems. It is undeniable that the initial starting design has a significant influence on the computational costs and the analysis time. Here a helpful technique a multilevel algorithm is introduced. It can save computational costs and improve the problem solving efficiency. This algorithm is achieved by firstly solving the problem on a coarse mesh to get a coarse material layout design with cheap computational costs. Then this coarse design is used as the initial starting design on a finer mesh in next level optimization problem. The steps may repeat several times until a desirable optimal design is achieved. By using multilevel techniques, unnecessary and expensive iterative computations on very fine meshes are avoided; which saves considerable analysis time.

In this chapter, three levels of a canyon bridge problem are solved in both multilevel cases and as single level cases. The total solving time is recorded for both cases to confirm the efficiency of multilevel techniques. Objective function graphs respect to iteration number are discussed.

3.1 Reduction Method

In solving bridge design problem, one quickly find that long span bridges are very sparse structures in the sense that their volume of structural material relative to the bounding volume of the bridge is very small. Especially in large-scale civil engineering structures such as long-span bridges and transmission towers, the results are characteristically very sparse with the volume of material that comprises the structural system constituting a very small fraction of the structure's total envelope volume. For a

sparse structure, the volume of material forming the structural system usually constitutes no more than 5% of the total design volume.

The Golden Gate Bridge in San Francisco is an example of a very the long-span sparse structure. The bridge towers are 230 meters tall and 27 meters wide and the bridge length is approximately 1970 meters. A bounding box with dimensions $230m \times 27m \times 1970m$ has a volume of approximately $12,200,000\text{m}^3$ (see dash box in Figures 3.1(b)). The construction of the bridge is reported to have used up to $75,300,000\text{kg}$ of steel ($9{,}600\text{m}^3$) and $297,000\text{m}^3$ of concrete (Golden Gate Bridge, Highway and Transportation District, 2012). Thus an approximation of the structural volume occupancy can be calculated by dividing the volume sum of both steel and concrete by the box volume: $(9,600+297,000)/12,200,000=2.5\%$. The volume occupancy of the Golden Gate Bridge is thus approximately 2.5% which is considerably smaller than that of other structures, such as buildings. With this high sparsity these structures require fine computational meshes to represent the distribution of material and to calculate the structural response, leading to significant computational intensity.

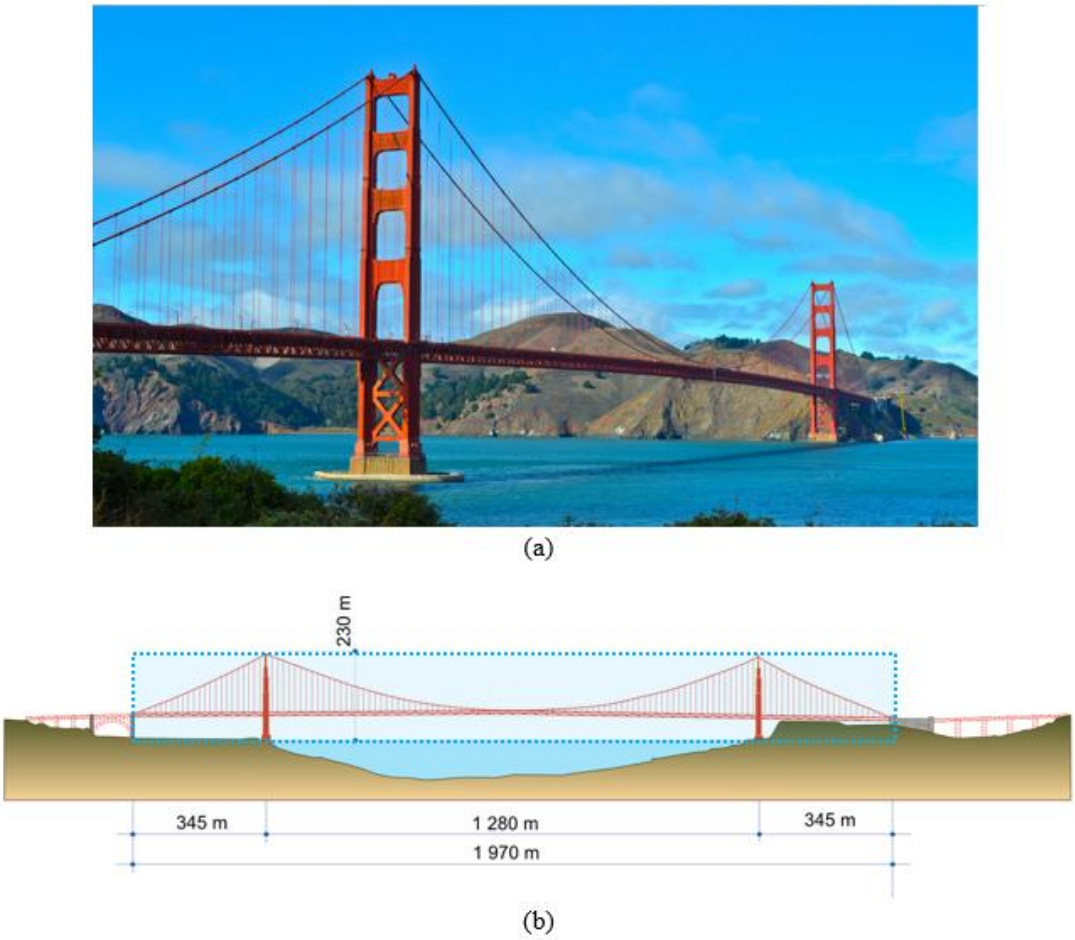

Figure 3. 1: An example for sparse structure: The Golden Gate Bridge in San Francisco (Edginton, 2013) with a design volume box added.

When dealing with continuum topology optimization of sparse structures using nonlinear analysis techniques (Rahmatalla and Swan, 2003) geometrical instability is one

of the critical problems that appears commonly. In a continuum structural system analysis, geometrical instability can lead to finite deformation which would cause numerical difficulties. The area with low stress or low sensitivity tends to come out with void and low-density elements. Deformations are quite large in this area due to the low stiffness of these void and low-density elements. Large-scale and sparse civil engineering structures results in large regions with finite deformation and structural instability. It is beneficial if the void and low-density elements in those regions can be removed temporarily from consideration during the structural analysis. This is called analysis problem size reduction and it is able to identify the void and low-density regions and remove temporarily the elements therein using an automated algorithm. It is noted that this robust algorithm only temporarily removes low-density regions as they are still present in the optimization problem and thus still able to become high density regions.

The analysis problem size reduction technique can be described in three simple steps.

1. The elements in the structure with solid volume fraction values equal to or less than 0.002 are determined as the "void" elements.
2. The nodes which are only members of "void" elements are identified as "prime" nodes.
3. The elements which are comprised only by "prime" nodes are marked as "prime" elements. Then such "prime" elements are removed during the structural analysis to avoid creating singularities of finite element equations (Figure 3.2).

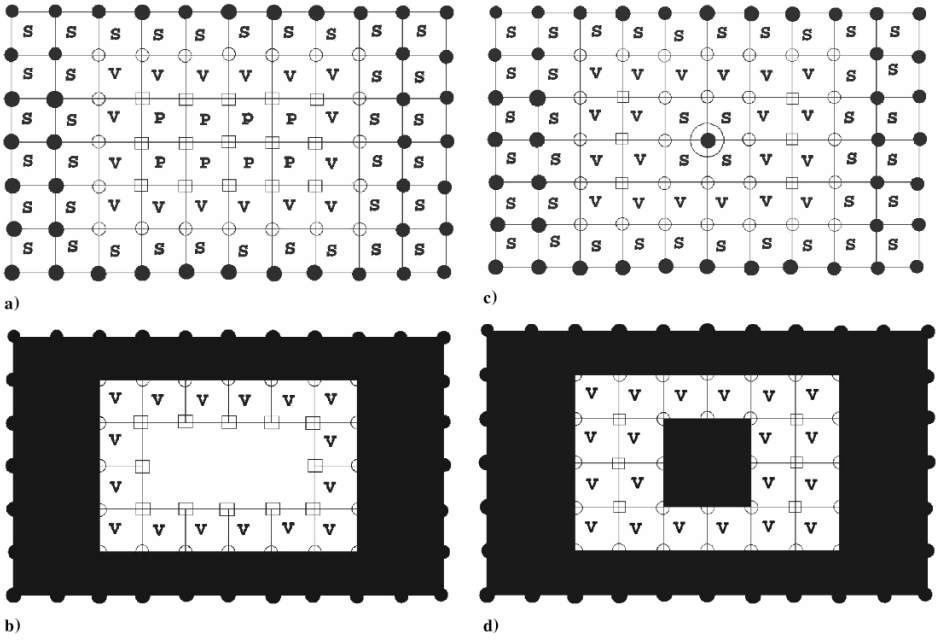

Figure 3. 2: Graphical examples description of size reduction technique (Rahmatalla and Swan, 2003).

Figure 3.2 are two examples demonstrating application of the size reduction method. Nodes with associated design variable values of zero are open circles; filled circles represent nodes with nonzero design variable values; nodes with open squares denote "prime" nodes whose degrees-of-freedom are restrained; elements with "S" are at least partially solid; elements with "V" are essentially devoid of solid material; elements with "P" are prime elements removed from consideration. Figures 3.2 (a) shows a mesh with designated nodes and elements while Figures 3.2 (b) shows the corresponding mesh used in analysis with solid elements blackened, prime elements removed, and void elements retained. Figures 3.2 (c) and (d) show another mesh with an isolated solid node surrounding by a region of void nodes, and the corresponding resulting mesh in which

there are no prime elements removed, thus avoiding formation of an island that is disconnected from the remainder of the mesh (Rahmatalla and Swan, 2003).

To avoid numerical difficulties and speed up the optimization process, this method is typically employed in all the computations of this study.

3.2 Problem Statement

Compliance minimization problems are solved for optimal material distributions of a canyon bridge model subject to constraints on the volume of structural material. The design domain is a rectangular region 1000 meters long by 500 meters high. Half of the nodes along the left and right boundaries are fixed. The bridge is carrying a 10kPa traffic load along the span at the deck level as shown in Figure 3.3.

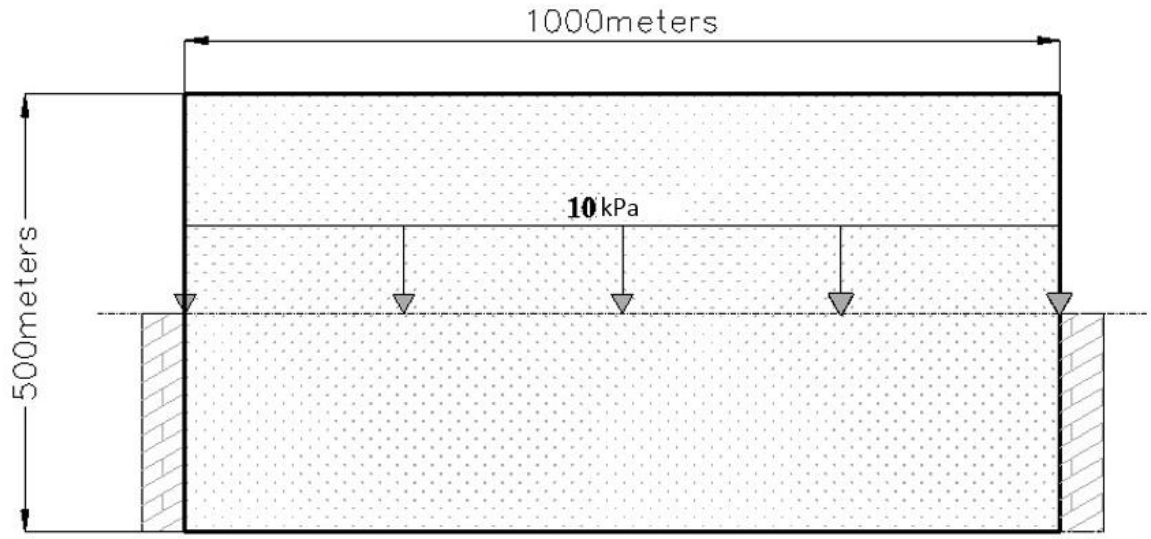

Figure 3. 3: Design region and applied set of loads.

The structural optimization is performed in two dimensions within a 1000 meter by 500 meter design region, which has a gross volume of 500, $000\,m^3/m$. Since the structural form is desired to be sparse, the structural material volume constraint is set to less than or equal to 5% of the bridge envelope volume ($0.05*500,000m^3/m$) or $25,000m^3/m$. Assuming that the main material for the bridge construction is steel, then the weight of this bridge would be ($0.078MN/m^3 \times 25,000m^3/m$)$1950MN/m$. It is thus apparent that the weight of the bridge is very large compared to the traffic load $10kPa \times 1000m=10MN/m$. It has previously been studied (Swan et al, 1998) that if self-weight is considered during the optimization process, it would be dominant and cause unsatisfactory concept designs. Therefore the self-weight is neglected during the topology optimization process and would be taken into consideration with traffic load only after the design structural forms are obtained.

The canyon bridge problem is solved on three levels of meshing. Level 0 mesh consists of totally 1800 elements which is of 60 elements by 30 elements, and each higher level would double the elements on each side of rectangle domain. Thus, there are 7200 elements for level 1 mesh and 28800 elements for level 2 mesh. The single element side length for three levels are 16.7 meters, 8.3 meters and 4.2 meters respectively. For the single level case all designs began with a solid structural domain. The multilevel case, only the level 0 problem began with a fully solid initial design, and the level 1 and level 2 problems began with the design layout results from lower level problems.

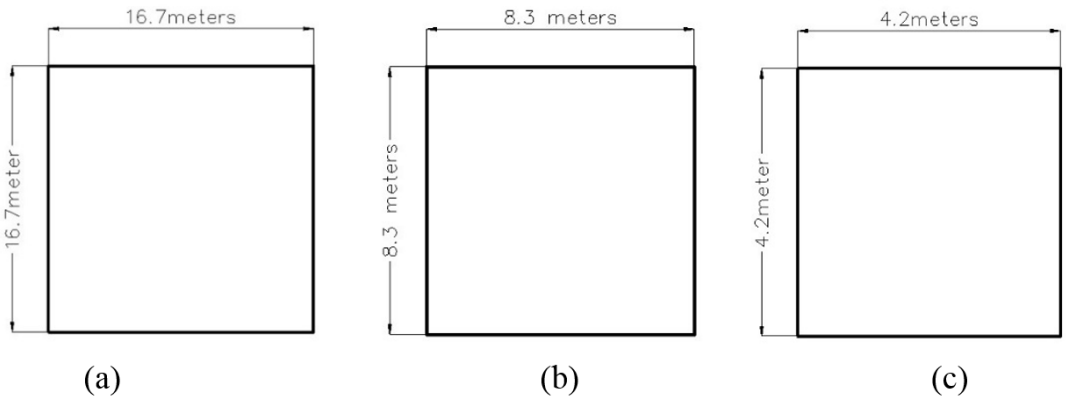

Figure 3. 4: Single element size. (a) Level 0. (b) Level 1. (c) Level 2.

Sequential linear programming is used to solve the optimization problem in mathematical iteration step. To analyze this canyon bridge problem considered as a quasi-static problem, and 2-D bilinear continuum quadrilateral element is used to solve momentum balance equation. The material steel is assumed to be isotropic with bulk modulus of 362 GPa and shear modulus of 118 GPa. In this topology optimization problem the model is treated as linear elastic.

Since there is only external force applied but no applied displacement, the second terms in equation 2.3 ($\min_b[\mathrm{M}(\mathbf{u},\mathbf{b}) = \frac{1}{2}(\mathbf{f}^{ext}\cdot\mathbf{u} + \sum_{E\in\eta_g}\mathbf{f}_{\mathrm{E}}^{\mathrm{int}}\cdot\mathbf{g}_E)]$) vanishes, and the problem formulation can be stated as:

$$\min_b\left[\mathrm{M}(\mathbf{u},\mathbf{b}) = \frac{1}{2}\mathbf{f}^{ext}\cdot\mathbf{u}\right] \tag{3.1}$$

subject to the volume constraint,

$$g_1 = \langle \phi_{\text{solid}} \rangle - C \leq 0 \tag{3.2}$$

Note $\langle \phi_{\text{solid}} \rangle = \frac{1}{V} \int_{\Omega} \phi \, d\Omega$

2.3 Sensitivity Analysis

The design problem is considered as an optimization problem in the design variables only and the displacement field is regarded as a function of these design variables. Finding the derivatives of the displacements with respect to design variables is termed sensitivity analysis. Since it is a single-objective problem with a minimum compliance, from equation (3.1) the design gradient of the objective function is computed.

$$\frac{dM}{d\mathbf{b}} = \frac{1}{2}\left(\frac{d\mathbf{f}^{ext}}{\partial \mathbf{b}} \cdot \mathbf{u} + \mathbf{f}^{ext} \cdot \frac{\partial \mathbf{u}}{\partial \mathbf{b}} \right) \tag{3.3}$$

Since $\mathbf{f}^{ext}$ is constant and independent of the design variables, the first term on the right hand side vanishes.

$$\frac{dM}{d\mathbf{b}} = \frac{1}{2}\mathbf{f}^{ext} \cdot \frac{\partial \mathbf{u}}{\partial \mathbf{b}} \tag{3.4}$$

$$\mathbf{r}(\mathbf{u}, \mathbf{b}) = \mathbf{K} \cdot \mathbf{u} - \mathbf{f}^{\text{ext}} = \mathbf{0} \tag{3.5}$$

$$\frac{d\mathbf{r}}{d\mathbf{b}} = \frac{d\mathbf{K}}{d\mathbf{b}} \cdot \mathbf{u} + \mathbf{K} \cdot \frac{d\mathbf{u}}{d\mathbf{b}} = 0 \tag{3.6}$$

$$\frac{d\mathbf{u}}{d\mathbf{b}} = -\mathbf{K}^{-1} \cdot \frac{d\mathbf{K}}{d\mathbf{b}} \cdot \mathbf{u} \tag{3.7}$$

Substitute (3.8) into (3.4), we have

$$\frac{dM}{d\mathbf{b}} = -\frac{1}{2}\mathbf{f}^{ext} \cdot \mathbf{K}^{-1} \cdot \frac{d\mathbf{K}}{d\mathbf{b}} \cdot \mathbf{u} \tag{3.8}$$

$$\frac{dM}{d\mathbf{b}} = -\frac{1}{2}\mathbf{u} \cdot \frac{d\mathbf{K}}{d\mathbf{b}} \cdot \mathbf{u} \tag{3.9}$$

$$\frac{dM}{d\mathbf{b}} = \mathbf{u_a} \cdot \frac{\partial \mathbf{f}^{\mathbf{int}}}{\partial \mathbf{b}} \tag{3.10}$$

$\mathbf{u_a}$ represents a vector of adjoint displacements which satisfies $\mathbf{K} \cdot \mathbf{u_a} = -\frac{\partial M}{\partial \mathbf{u}} = -\frac{1}{2}\mathbf{f}^{ext}$.

$$\mathbf{f}^{int} = \int_{\Omega} \mathbf{B}^T \boldsymbol{\sigma} d\Omega \tag{3.11}$$

$$\mathbf{f}^{int} = \int_{\Omega} \mathbf{B}^T \mathbf{E}(\mathbf{b}) \cdot \boldsymbol{\varepsilon} d\Omega \tag{3.12}$$

where $\mathbf{B}$ represents the strain displacement matrix and $\boldsymbol{\varepsilon}$, $\boldsymbol{\sigma}$ are the strain and the stress which are both in a condensed form:

$\boldsymbol{\varepsilon} = (\varepsilon_{11}, \varepsilon_{22}, \varepsilon_{33}, \gamma_{23}, \gamma_{13}, \gamma_{12})$; $\boldsymbol{\sigma} = (\sigma_{11}, \sigma_{22}, \sigma_{33}, \sigma_{23}, \sigma_{13}, \sigma_{12})$. $\mathbf{E}$ is the modulus which is condensed into a 6×6 matrix. Substitute (3.13) into (3.11), we have

$$\frac{dM}{d\mathbf{b}} = \mathbf{u_a} \cdot \frac{\partial}{\partial \mathbf{b}} \left(\int \boldsymbol{B}^T \mathbf{E}(\mathbf{b}) \cdot \boldsymbol{\varepsilon} d\Omega \right) \tag{3.13}$$

$$\frac{dM}{d\mathbf{b}} = \mathbf{u}_a \cdot \int \boldsymbol{B}^T \frac{\partial \mathbf{E}(\mathbf{b})}{\partial \mathbf{b}} \cdot \boldsymbol{\varepsilon} d\Omega \tag{3.14}$$

$$\frac{dM}{d\mathbf{b}} = \int \boldsymbol{\varepsilon}_a \cdot \frac{\partial \mathbf{E}(\mathbf{b})}{\partial \mathbf{b}} \cdot \boldsymbol{\varepsilon} d\Omega \tag{3.15}$$

3.2 Resulting layouts

As the meshes are refined, the constraints on the volume of structural material are gradually tightened as indicated in Table 3.1 where V denotes the design region.

Table 3. 1: Volume restrictions on structural material for three mesh levels.

l	Level 0	Level 1	Level 2
Volume constraint C	$0.2V$ $5,000m^3/m$	$0.1V$ $2,500m^3/m$	$0.05V$ $1,250m^3/m$

For a multilevel problem, the resulting layouts for three levels are shown in Figure 3.5. The level 0 mesh problem is solved until the solution is feasible which means that the maximum constraint violation vanishes. The design solution is then transferred to the level 1 mesh where the process continues for 50 iterations after the solution becomes feasible once again. The level 1 solution is then transferred to the level 2 mesh where

optimization iterations continue until an optimum is achieved. The reason for using different stopping criteria on the lower level meshes is that goal on the lower level problems is to take out most of the material from the domain and show a very general material arrangement. In other words the coarse mesh problems are only auxiliary and their results don't need to be highly accurate. Accordingly the stopping criterion of feasibility on the lower levels can reduce the optimization time. Figure 3.5 shows that the resulting layouts on each level clearer are getting clear with mesh refinement The actual material layout ends up with a through arch bridge.

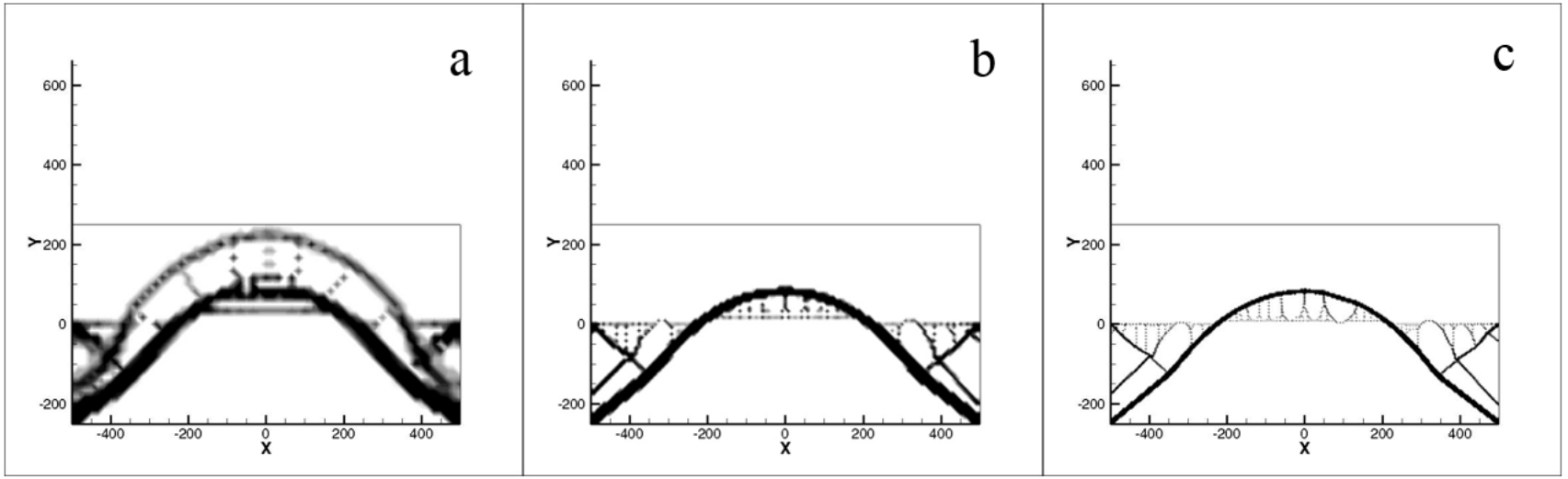

Figure 3. 5: Layout solutions with multi-level refinement. (a) Level 0: Starts with solid design; runs until feasible. (b) Level 1: Starts with level 0 resulting design; runs 50 iterations after problem being feasible. (c) Level 2: Starts with level 1 resulting design; runs until optimal design achieved.

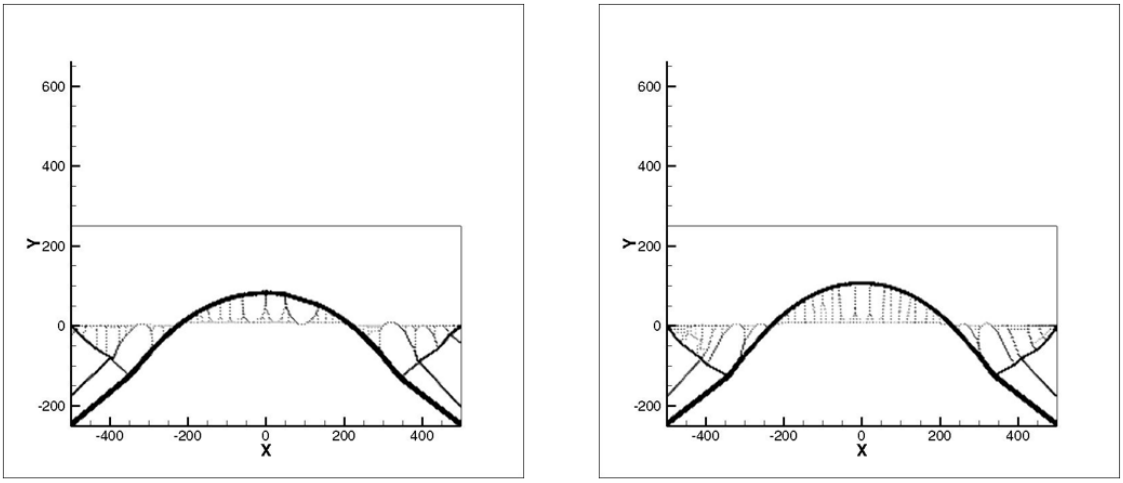

Figure 3. 6: Comparison: Multilevel solution and single level solution for level 2 mesh. (a) Multilevel problem: Starts from level 1 resulting design and continues to optimality; (b) Single level problem starts from solid design and continues to optimality.

The multilevel solution from Figures 3.5 (c) is compared with a single level solution on the level 2 mesh in Figure 3.6. As can be seen from the comparison, two layout results achieved very similar structures. They are basically layouts of a compression arch with a slender deck passing through. The single level solution has more tensile members above the center of the deck. In addition, the arch in multilevel solution has a larger radius of curvature which is about 50 meters larger than that in single level. The rise of the arch in the multilevel solution is smaller than that of single level solution and thus has a larger span to rise ratio. From Table 3.2 shown as follow, it can be found that the object function values are pretty close. This similarity indicates that the method

of multilevel algorithm implementation in optimization has a very slight influence on the resulting layouts.

Table 3. 2: Objective functions for multilevel solution and single level solution

Problem Type	Objective function value $F_o\left(kN \cdot m\right)$
Multilevel problem	3.11E+05
Single level problem	3.27E+05

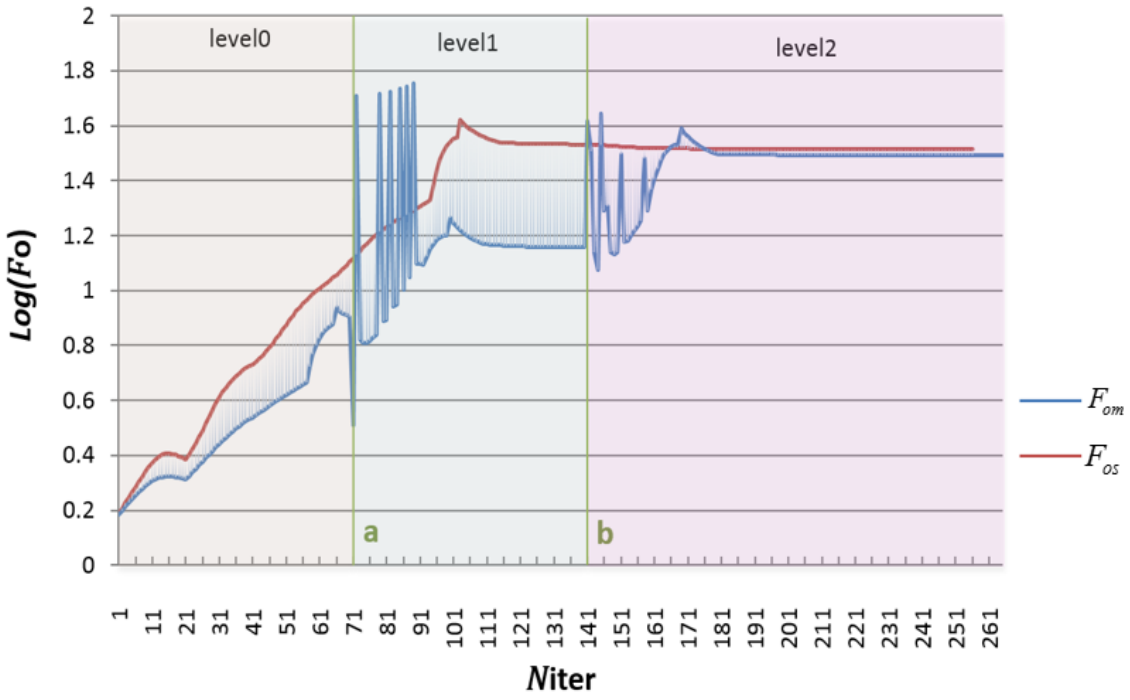

Figure 3. 7: Results curves: objective function history with respect to iteration counts. F_{om} and F_{os} represent objective function for multilevel solution and single level solution.

Figure 3.7 shows objective function value curves for both multilevel case and single level case. To better evaluate, the logarithm of objective function value with the base of 10 is used for showing smoother curves. During the process of iteration, F_{os} and F_{om} start from a same point which is a corresponding F_o value based on a complete solid design. Then curve of F_{os} goes higher than that of F_{om} which is caused by different volume restrictions in two cases. As the designs gradually get to converge, the gap between those two curves narrows. Eventually two function values stabilize and the curves stay very close to each other. The reason is that multilevel level 2 problem is solved with a volume restriction same as the one in single level problem. Around

iteration 20, each curve is having a peak which reflects that those two cases may experience a similar problem of optimization computation.

By taking a close look at F_{os} curve, one can find out that the curve keeps going up until iteration 110, though the goal of the problem is to find a minimum cost function in which a decreasing value is prefered. This is because the problem is having an initial design of whole solid structure over the design region, which possesses a stiffer structural behavior but not satisfies the volume constraint. Thus, in the first place of the iteration, the computation works on taking out material to make the problem feasible, however, which would result in a decreasing of the stiffness (an increasing of the compliance) in the structure. As the curve reaches a peak (feasible peak), the problem gets feasible and the computation aim turns to find a minimum cost function value. It also well illustrate the appearance of three feasible peaks in curve F_{om}. Multilevel problem is solved on three levels of mesh thus experiences feasible for three times.

Besides, around iteration 70 and 140, curve of F_{om} experiences significant jumps, however, there is no such fluctuation for F_{os}. Instead, the curve for F_{os} is very smooth around that period of iterations. It is obvious that this period is the beginning of level 1 mesh optimization. And another period from iteration 140 to 170 being the beginning of level 2 mesh optimization are also experiencing oscillations in the cost function. During these two period, two conditions change when a coarse mesh problem goes into a finer mesh problem. One is the volume constraint upper bound which reduced by half; and another is the total elements in the design domain which would quadruple. By taking a close look at the objective function：

$$M = \frac{1}{2}\mathbf{f}^{ext} \cdot \mathbf{u}$$

Where $\mathbf{f}^{ext}$ is a constant in the problem and would not change by neither the smaller volume constraint upper bound nor the total element number. While displacement $\boldsymbol{u}$ would increase in the first iteration in a new level computation for the reason that finer mesh helps reducing the finite element error. In finite element analysis, the displacement being calculated in coarse mesh would underestimate the actual situation. After each refinement step, the error in a fine mesh is strictly smaller than the error in a coarse mesh. It well illustrates the jump performance in $F_{\text{om}} - N_{\text{iter}}$ curve.

To verify the influence caused by the changing in volume restriction, additional optimizations are solved in level 0 and level 1 mesh problems with a volume constraint upper bound of $5\%\,\text{V}$ which is same as the one in level 2 problem. However the oscillations remain. It proves that the mesh refinement is the cause of this problem.

3.3 Total analysis time

If it is certain that problem using multilevel algorithm can result in convincing design layout, then how efficient can it work to help with the reduction of computation costs? Here a time counter is added to problem. The total computation time is consists of time used for finite element analysis, the solution of SLP, and system connection. Since system connection time are variable in different conditions and SLP optimization time doesn't have obvious change by element number, the summation of finite analysis time in each iteration is recorded in this study to make a comparison between two problems shown in Table 3.3. Where N_{e} and N_{iter} represent the number of element and iteration needed in each problem respectively. t_{a} and t_{ave} with the unit of seconds are the summation of finite analysis time and the average time in one iteration.

It is important to notes that N_{iter} and t_{a} for single level case are the exact iteration and time taken in each level computation; however for multilevel case, N_{iter} and t_{a} are entered as the total time and iteration needed since the optimization starts from a solid

design (from level 0) instead of the one needed in each level computation. The computations were performed on a computer with a 3.4 GHz CPU and 16 GB memory.

Table 3. 3: Problem computation comparison

l	N_e	Single level			Multilevel		
		N_{iter}	t_a	t_{ave}	N_{iter}	t_a	t_{ave}
Level0	1800	70	5.42	7.75E-02	70	5.42	7.75E-02
Level1	7200	90	50.8	5.65E-01	140	17.4	1.24E-01
Level2	14400	256	359	1.40E+00	275	111	4.07E-01

In single level case, level 0 and level 1 problems stopped iterating when optimal points achieved, while in multi-level case, level 0 problem ran till the design is feasible and level 1 iteration stopped 50 iterations after problem feasible. It can be found that even though multilevel problems did less work on the progress to achieving optimal design, the number of iteration needed is close to or even greater than that in single level problem.

Since iteration number needed is a minor concerned aspect and it is the analysis time that is sensitive to the computational intensity, more results analysis is made based on computational time. The level 0 computations for both cases are exactly the same

since they all started form a solid design. The refinement began in level 1. In this level, t_{ave} of single level case is over 4 times as that of multi-level case. And in the next level, single level case analysis time is 359.065 seconds which is about 3 times as the time multi-level problem needed. The time saving is over 240 seconds. From those data, it is convincing that by using multilevel algorithm together with reduction method, computational effort saving is remarkable. When dealing with a very fine mesh or a 3d problem, the computational costs would increase dramatically. However in those problems multilevel refinement would show higher performance which can bring out considerable computation saving.

3.4 Perimeter constraint

To alleviate the mesh-dependency problem and the checkerboard patterns in this canyon bridge problem, additional optimization problems are solved with a perimeter constrain enforced. Thus the problem can be stated as:

$$\min_{b}\left[M\left(\mathbf{u},\mathbf{b}\right)=\frac{1}{2}\mathbf{f}^{ext}\cdot\mathbf{u} \right]$$

Subject to, (3.16)

$$\mathrm{g}_1=\phi_{\text{solid}}-C\le 0$$

$$\mathrm{g}_2=\mathrm{P}\left(\mathbf{b}\right)-P_u\le 0$$

Where, $\mathrm{P}\left(\mathbf{b}\right)$ represents the perimeter of the design structure; P_u represents the upper bound constraint value on the design perimeter. Apparently, the smaller the upper bound constraint value is, the coarser design results would be attained.

Firstly, for the perimeter constraint, an upper bound of three times the design domain perimeter is introduced to the problem (P_u =3* P_{domain} =3*(1000+500)*2=9000 meters). The design result for level 2 mesh in single level solution is shown as follow:

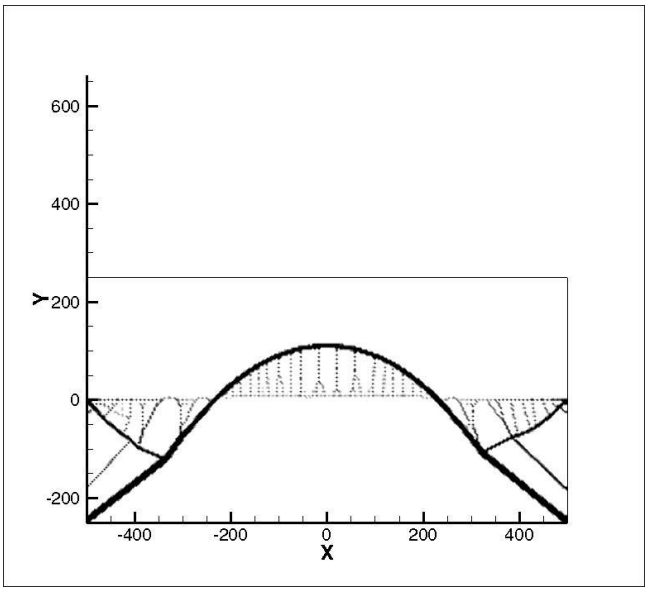

Figure 3. 8: Single level: Level 2 mesh with perimeter constraint.

Table 3. 4: Single level: level 2 mesh with perimeter constraint of $3^* P_{domain}$; starting from a solid structural design initially.

l	$F_o(kN \cdot m)$	$g_1 = \phi_{solid} - C$	$g_2 = P(\mathbf{b}) - P_u \le 0$
Single-level	3.27E+05	4.58E-16	-1.23E+03

The numerical results above show that the structure compliance reach a value of 32.7 with only one constraint function value nearly zero, however the perimeter constraint function with value of -1230 is far from feasible. In an optimization problem, in order to alleviate the numerical instabilities efficiently, an active perimeter constraint function is strongly expected.

$$g_2(\mathbf{b}) = P(\mathbf{b}) - P_u = -1230 \tag{3.17}$$

$$P(\mathbf{b}) = g_2(\mathbf{b}) + P_u = 7770 \tag{3.18}$$

A structure design perimeter of 7770 meters smaller than the upper bound P_u (9000 meters) is got, which means that the perimeter constraint function newly introduced does not restrict the design perimeter effectively. Thus, a tighter limit smaller than 7770 meters is needed. The perimeter constraint upper bound P_u is then reduced from 9000 meters to 6000 meters which is two times the design domain perimeter. Since

the constants in the second constraint function is comparatively large with that in volume constraint. To better evaluate two constraint function values, two scalar constants, CVAL and SVAL are introduced to the perimeter constraint function. The new constraint function becomes:

$$g_2 = \mathrm{P}(\mathbf{b}) * [\mathrm{SVAL}] - [\mathrm{CVAL}] \tag{3.19}$$

Where $[\mathrm{SVAL}]=1.0E-4$, $[\mathrm{CVAL}]=[\mathrm{SVAL}]*P_u=6.0E-4$

$$g_2 = 10^{-4} * \mathrm{P}(\mathbf{b}) - 6.0 * 10^{-4} \tag{3.20}$$

The resulting layouts show as follow:

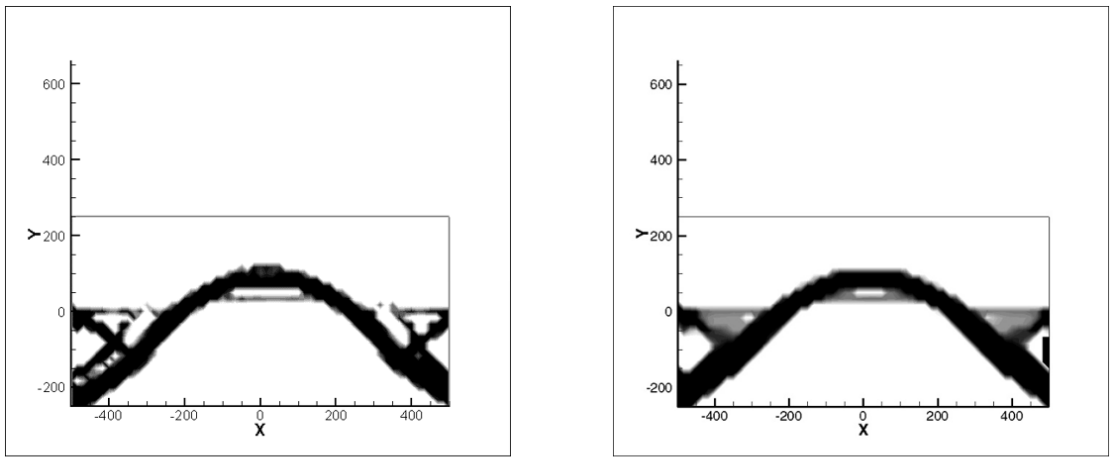

Figure 3. 9: Single level: Level 0 optimization design. (a) Without perimeter constraint M= 6.32E+04. (b) With perimeter constraint M= 6.26E+04

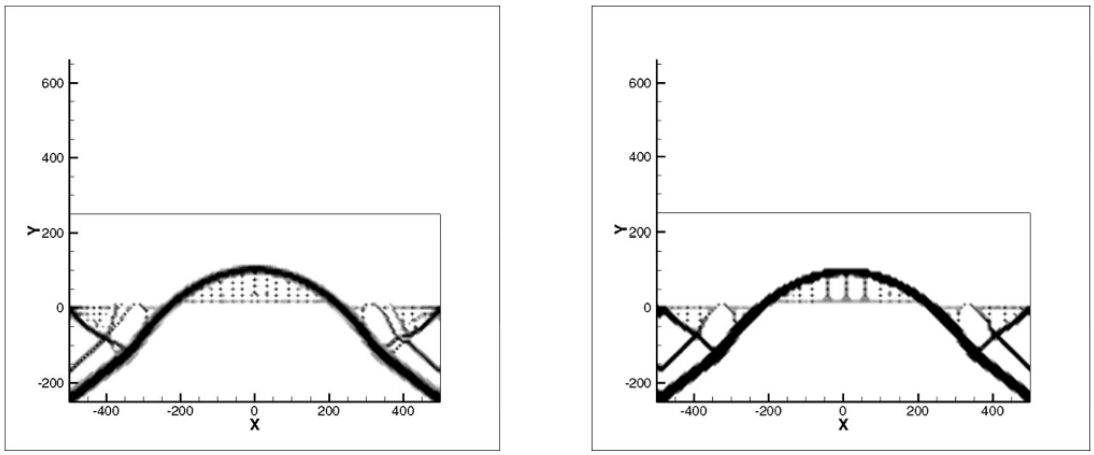

Figure 3. 10: Single level: Level 1 optimization design. a) Without perimeter constraint M= 1.61E+05. b) With perimeter constraint M=1.42E+05.

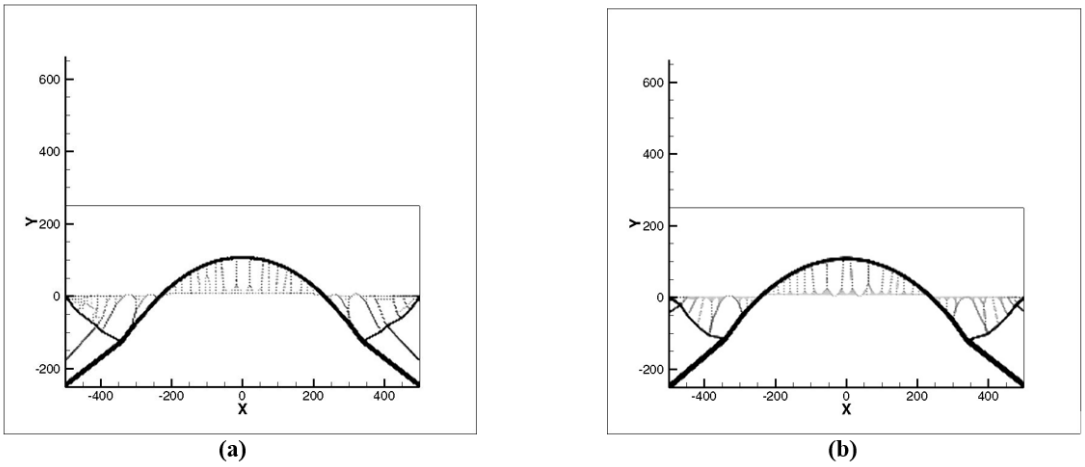

Figure 3. 11: Single level: Level 2 optimization design: (a)Without perimeter constraint M= 3.27E+05. (b) With perimeter constraint M= 3.20E+05.

As shown above, the canyon bridge model was progressively refined in both direction uniformly. From Figures 3.9 (a) to 3.11 (a) shows the resulting layout solutions without perimeter constraint. The layout results in each level also feature non-convergent type design solutions due to having more complex designs in finer meshes around area of each end of the bridge deck. With an imposed perimeter constraint, the design solutions from Figures 3.9 (b) to 3.11 (b) are free of the "islanding" and "layering. Besides, the results of low level coarse mesh are nearly identical to that of high level fine mesh which shown a mitigation of mesh-dependency.

In Figure 3.12, the compression members supporting the deck (as signed with circle 1) tend to be simple and easy to interpret in the (a). And the supporting member signed with circle 2 is removed in design with perimeter control which makes the layout solution much easier to interpret and construct.

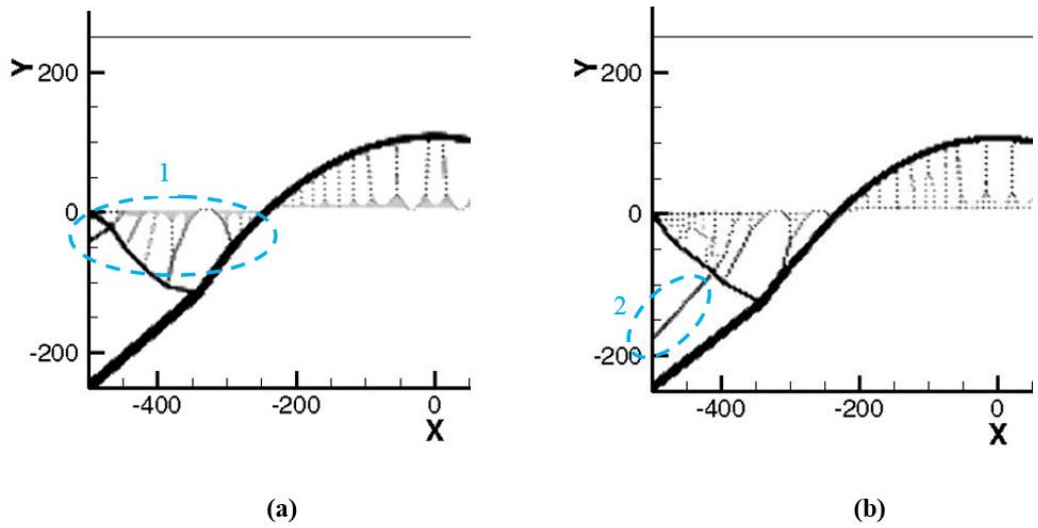

Figure 3. 12: Layout design detail comparison for single level solution level 2 mesh optimization. (a) With perimeter constraint (b) without perimeter constraint

Table 3. 5: Results: problem design results.

l	$F_o\left(kN\cdot m\right)$	$g_1=\phi_{solid}-C$	C	$g_2=P(\mathbf{b})-P_u$	[CVAL]
Level 0	6.26E+04	5.55E-17	20% V	1.11E-03	0.3
Level 1	1.46E+05	3.20E-16	10% V	2.46E-04	0.55
Level 2	3.20E+05	-1.73E-16	5% V	9.84E-04	0.6

For multilevel level 2 problem, an imposed perimeter constraint is introduced with the upper bound of two times the domain perimeter. The imposed constraint greatly increased the computation intensity and make it hard for the problem to converge. So convergence tolerance is loosed from 1.0E-7 to 1.0E-3 in this case. The results are shown in Table 3.6.

Table 3. 6: Problem analysis comparison for level 2 with perimeter constraint.

l	N_e	Single level			Multilevel		
		N_{iter}	t_a	t_{ave}	N_{iter}	t_a	t_{ave}
Level2	14400	320	421	1.32E+00	260	103.8	3.96E-01

From Table 3.6, it can be found that multilevel method has superiority on solving time for problems with perimeter constraint too. The average iteration time for multilevel case is about one third as that of single level case.

Compared to the data from Table 3.3, one can find that the analysis time for problems solved with or without perimeter constraint are close. However the clock time of problem solving for single level case is over 40 minutes long which is about 3 time as for the same problem without perimeter constraint. The reason is that SLP solving time increases a lot by adding another constraint.

In Figure 3.13 shows the resulting layouts of multilevel solution without and with perimeter constraint. Slight difference can be found between these two layouts which is unlike the single level case.

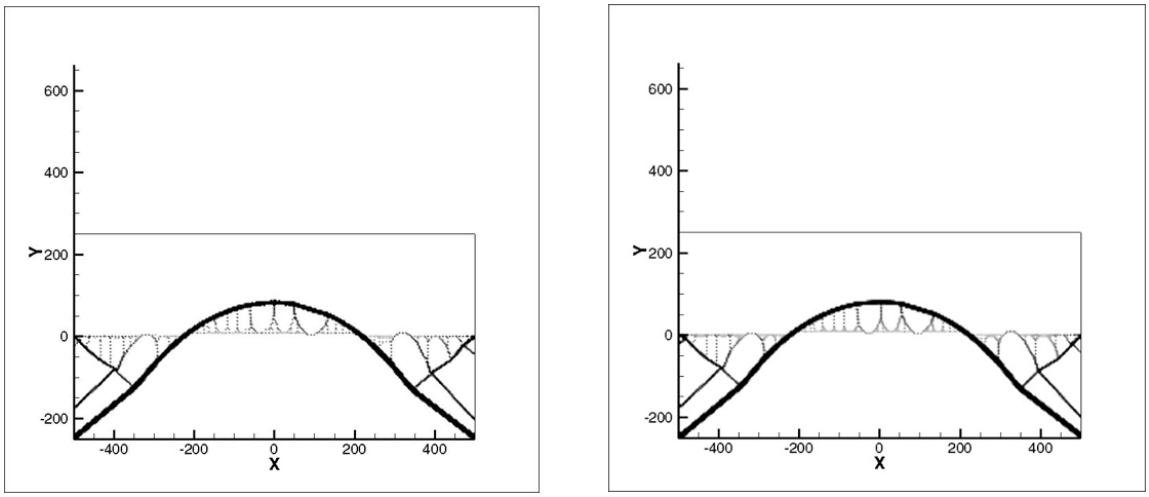

Figure 3. 13: Resulting layout: Multilevel problem without and with perimeter constraint

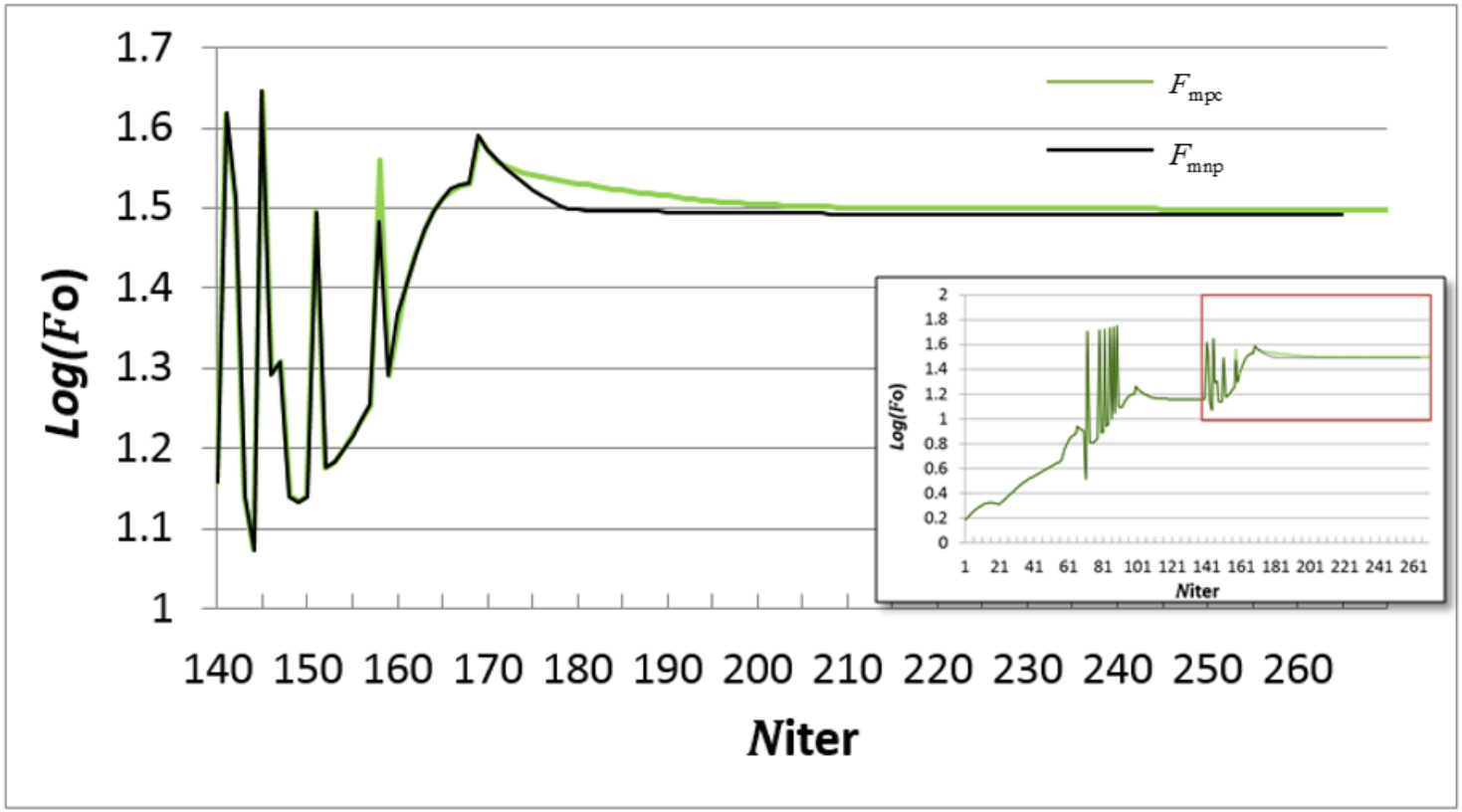

Figure 3. 14 : Curves Comparison: multilevel problem level 2 optimization. F_{mpc} represents the logarithm of objective function value for multilevel problem with a imposed perimeter constraint. F_{mnp} represents the logarithm of objective function value for multilevel problem without perimeter constraint.

In Figure 3.14 shows two curves of multilevel level 2 optimization. One is computed with perimeter constraint, however the other one is not. Before iteration 158 two curves are pretty close to each other, however in iteration 159 two curves separate at a steep peak. The value of F_{mpc} appears to be larger than that of F_{mnp} . After feasible peak around iteration 170, two curves stabilize but F_{mpc} is of a more moderate slope which means that it convergence slower than F_{mnp} does. The convergence feature of these two curves meets the fact that problem with perimeter constraint takes longer time and more iterations to convergence.

Since curves for multilevel solution with and without perimeter constraint are having slightly difference, only curve of F_{mpc} is taken into consideration in the next comparison curve diagram. In Figure 3.15, two single level level2 solution curves with the difference of with or without perimeter constraint are added. From the iteration beginning to iteration 40, curves of F_{spc} and F_{snp} almost coincide with each other. After iteration 40 the rising trend for F_{spc} becomes slower than that of F_{snp} . This phenomenon can also illustrate that perimeter constraint would slow down the optimization process. Then two curves reach their feasible peaks which sharing a same value, at iteration 103 and 152 respectively. Although as Figure3.16 shown two curves goes to a close value after the peaks, F_{spc} curve still has some un-neglected oscillations which makes it takes many more iteration to converge.

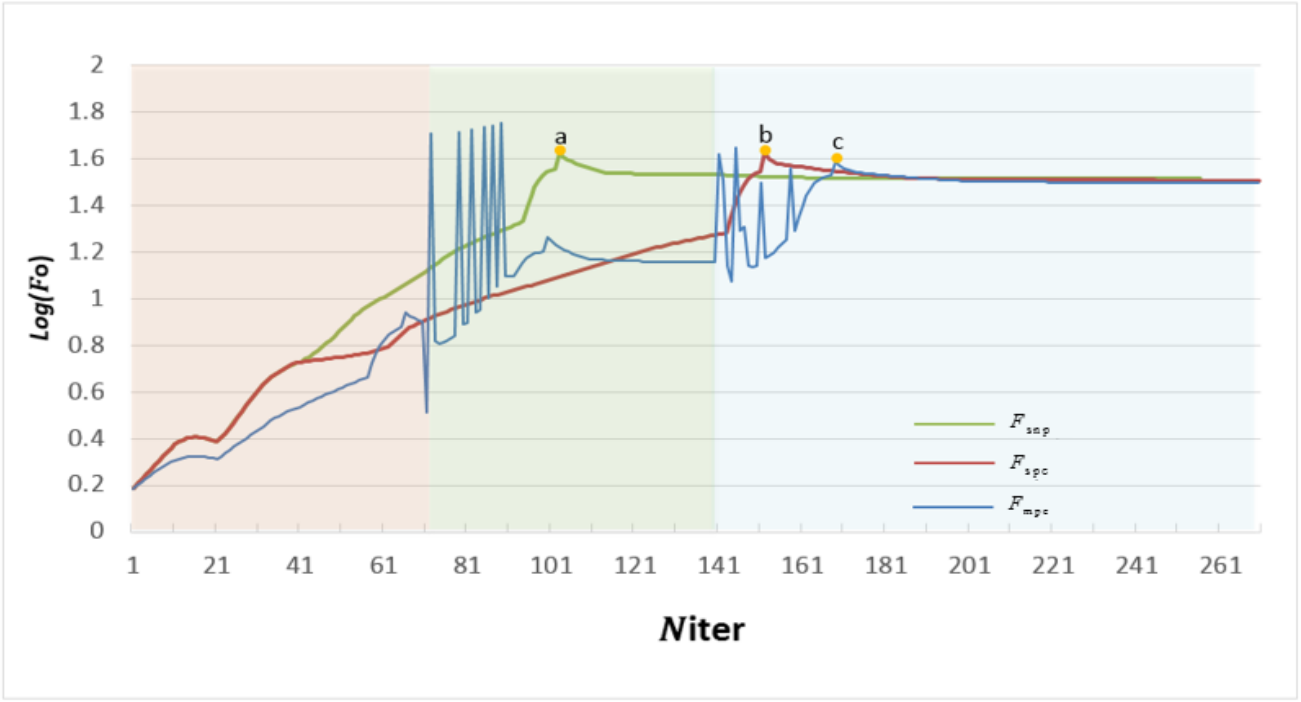

Figure 3. 15: Curves Comparison under three situations. F_{snp} represents the logarithm of objective function value for single level level 2 solution without perimeter constraint. F_{spc} represents the logarithm of objective function value for single level level 2 solution with a imposed perimeter constraint. F_{mpc} represents the logarithm of objective function value for multilevel solution with a imposed perimeter constraint.

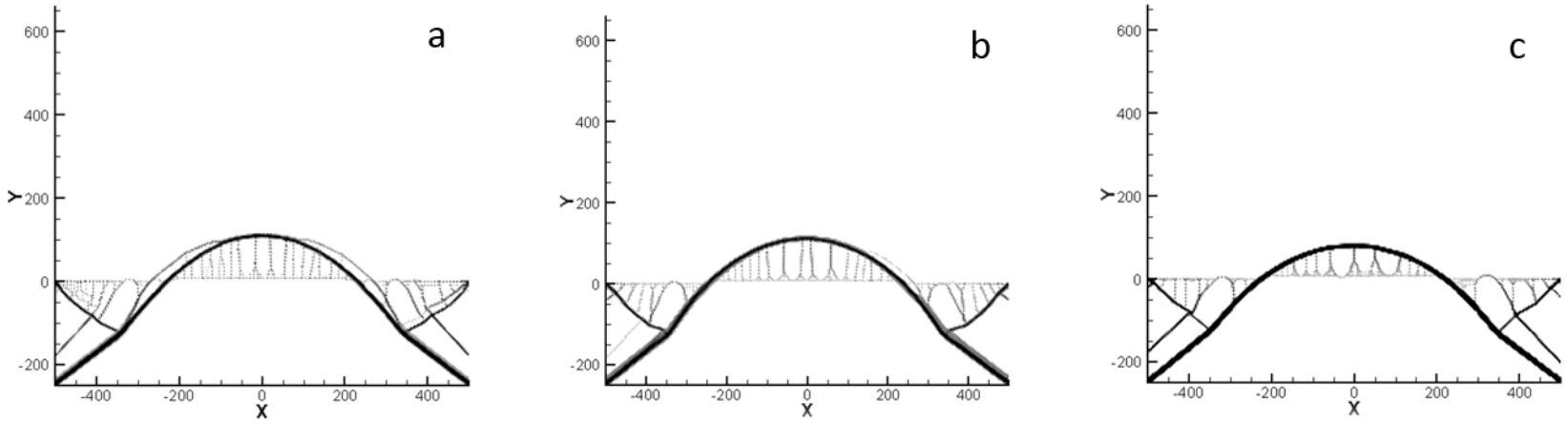

Figure 3. 16: Corresponding structural design layouts for point a, b, c in Figure 3.16. (a) Single level level2 problem without perimeter constraint. Iteration 103. (b) Single level level 2 problem with perimeter constraint. Iteration 152. (c) Multilevel level2 problem with perimeter constraint. Iteration 167.

Apparently at those three feasible peaks, three problems are experiencing a similar iteration progress. Their objective functions are all reaching the last maximum points before the curves go down and gradually approach the convergent value. In Figure3.15, the structural layout designs at the final peak for three curves are shown. From those layout design, it can be found that the optimization completeness for F_{mpc} is ahead of the other two problem on the optimization process, for the reason that the structural design is very close to the one in the final design. There would be slight changes on this design in the further iterations before the problem converges. Since Figure 3.16 (a) the layout shows one more arch addition to the final design arch , the optimization completeness F_{snp} lists bottom.

CHAPTER 4

SUMMARY AND FUTURE STUDY

4.1 Layout result evaluation and case study

La Vicaria Bridge is a through arch bridge in the Segura River, Spain. Although the lateral sides of the design boundary are slopes instead of vertical sides, the design of the arches and size proportion can provide ideas to better evaluate the topology optimization results.

The arches of La Vicaria Bridge span 168 m, of which 120 m is over the deck, with a 10 °inward incline towards the deck. The rise is 49 m, of which 25 m is over the deck. The span to rise ratio is 3.4:1. This bridge is a steel structure (arch and deck) which is same as the material of computation model.

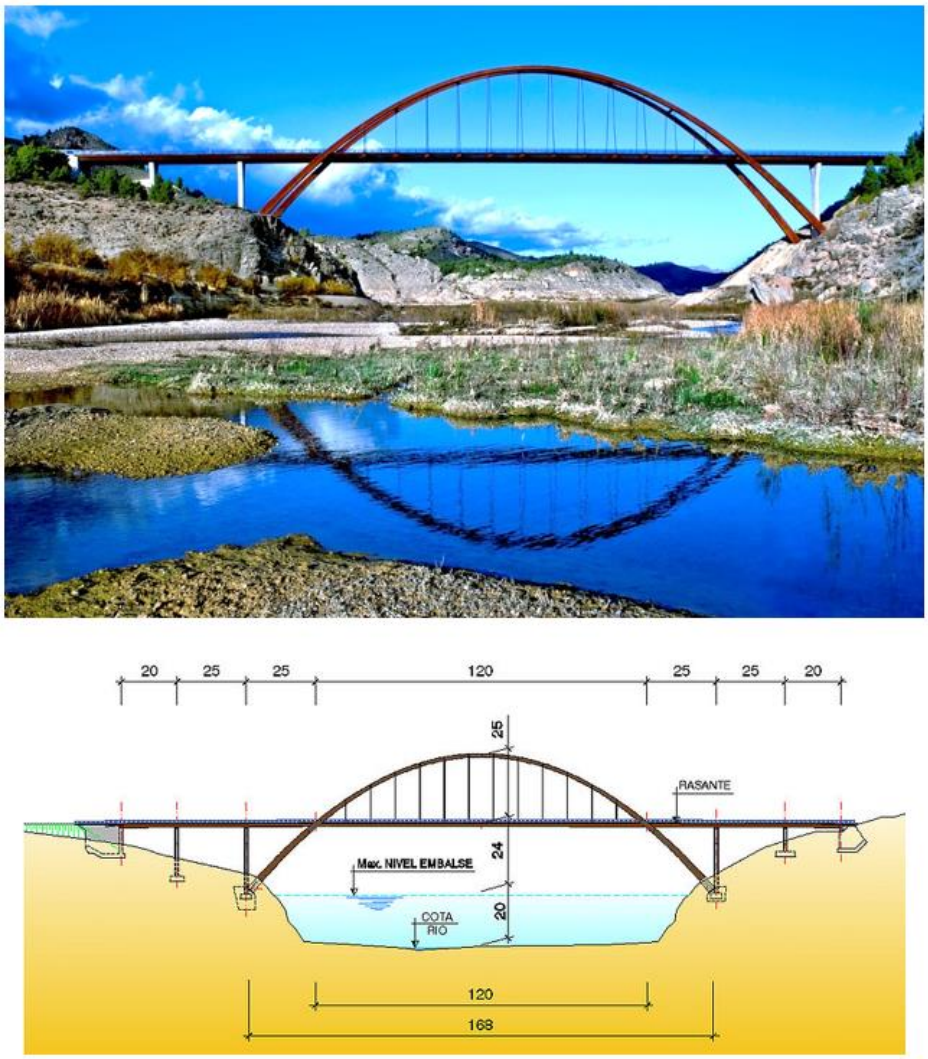

Figure 4. 1: La Vicaria Bridge, Albacete, Spain (Luis Martin-Tereso, 2008).

Figure 4.2 shows the resulting layout in single level level2 solution. The topology optimization results in a through arch bridge with a single arch which spans 1000m which is much greater than La Vicaria Bridge in case study. And 490m of the span is over the

deck. The arch covers a circular segment of 76° and with a radius of 400m.The rise is 350m, with 125m over the deck. The span to rise ratio is 2.9:1 and the elevation is about 38°.

Usually the arch bridge has an average span of 40m to 500m. For example, Chaotianmen Bridge, China is the arch bridge with longest span of 552m. However, the result design shows a long span arch bridge of 1000m which would lead to big self-weight and difficulty for construction. For a long-span bridge, buckling load is another crucial problem need to be considered except for structural stiffness. So by considering buckling load in this optimization, the optimization problem would come out more practical layout designs.

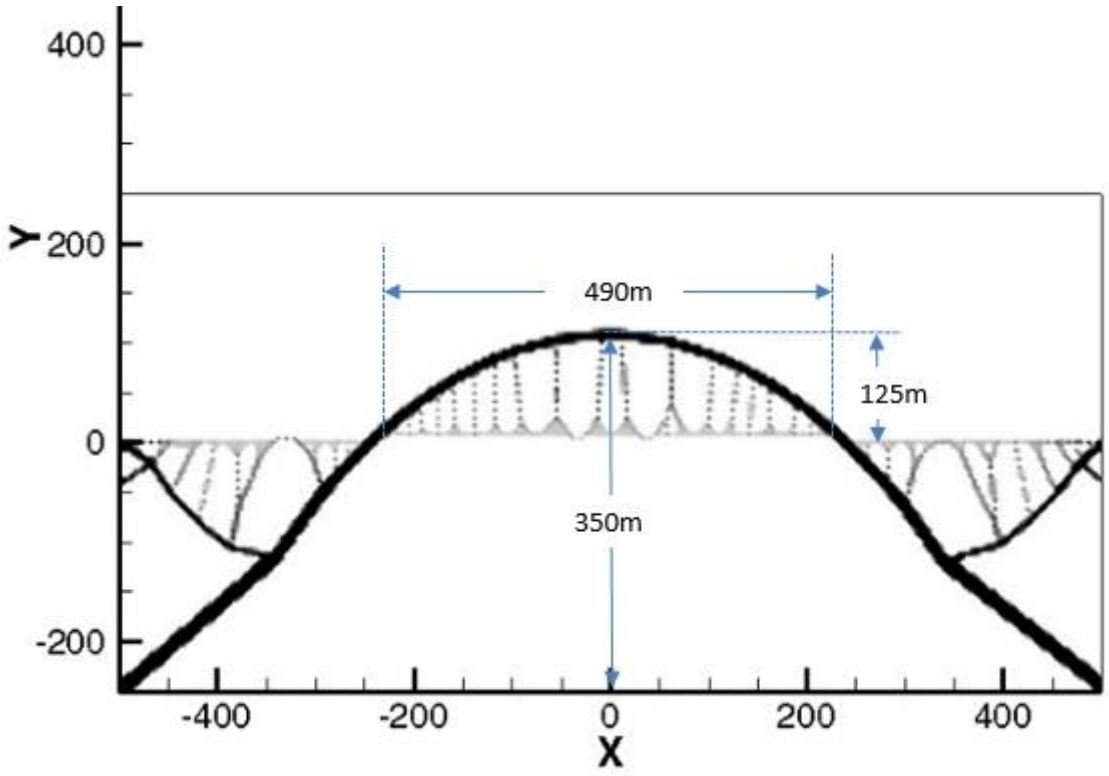

Figure 4. 2: A layout of structural design.

4.3 Conclusion

In this study, we attempted to reduce the computational intensity by applying both a multilevel algorithm and a reduction method. The proposed techniques are found in this study to reduce the computational effort required by a factor of about 3. Multilevel algorithm provides a considerable saving of computation effort and iteration time. Besides, the results solving by a multilevel problem shows great similarity with the ones

solving by a traditional single level problem. This proves the reliability for multilevel method.

4.3 Future Study

First of all, a finer mesh layout result is needed for the reason that the single element with the side of 4.2 meters is still quite large in size. Usually one single lane in highway is 3.6 meters (12 feet) which is smaller than the element in level 2 problem. If one element results in solid in an optimization problem, there would be an area of 4.2m by 4.2m (17.64m^2) or a three dimensional space of 74 m^3 in solid. However, by taking the main cable of the golden bridge as an example, the diameter is 0.92 m. It is obvious that the level 2 mesh is much too coarse to show a clear view of structural components in a bridge. Thus optimization computation on several higher level meshes are in great need to provide a much finer structural layout results.

Second, two dimensional results cannot satisfy the actual design demand, so 3D canyon bridge problem is another study that could be done in a further work. As for solving a three dimensional problem, the number of element would be increased exponentially when refine into a higher level design. For instance, assumes that 3D level 0 bridge model can be 2D problem extruding 80 meters in z direction, then it would have 60*30*5 (9000) elements. As for a 3D level 1 problem, the number of element in each direction should multiply by 2, then there would be 72,000 elements totally which is about 10 times as the elements for a 2D level 1 problem. 3D level 2 problem where computation intensity already appears during the solving process exists 576,000 elements which is 20 times as the elements in corresponding 2D problem. The multilevel algorithm can help a lot in saving the computational efforts in solving 3D problems.

REFERENCES

"Hite Country". Rmock.com. (2011). Retrieved from: http://www.rmock.com/trips/utah/hite.htm

Arora, J.S. (2012). Introduction to optimum design. McGraw-Hill(New York). ISBN 007002460X

Beghini, L. L. (2013). Building science through topology optimization (Doctoral dissertation). University of Illinois at Urbana-Champaign.

Bendsøe, M.P. (1989). Optimal shape design as a material distribution problem. Struct. Optim. 1, 193 –202.

Bendsoe, M.P., Sigmund, O. (2003). Topology Optimization-Basic Theory, Methods and Applications. Springer.

Browne, P. A. (2013). Topology optimization of linear elastic structures (Doctoral dissertation). University of Bath, Department of Mathematical Sciences.

Buhl, T., Pedersen, C.B.W., Sigmund, O. (2000). Stiffness design of geometrically nonlinear structures using topology optimization. Struct. Multidisc Optim. 19, 93-104.

Cai, K., Shi, J., Chen. B. S., Zhang, H. Z. (2008). Stiffness Design of Continuum Structures by a Bionics Topology Optimization Method. J. Appl. Mech. 75(5), 051006.

Deaton, J. D., Grandhi, R.V. (2014) A survey of structural and multidisciplinary continuum topology optimization: post 2000. Struct Multidisc Optim (2014) 49:1–38

Diaz, A., Sigmund, O. (1995). Checkerboard Patterns in Layout Optimization. Structure Multidisc Optimization 10:40–45

Fujii, D., Kikuchi, N. (2000) Improvement of numerical instabilities in topology optimization using the SLP method. Struct Multidisc Optim 19, 113-121.Springer-Verlag 2000.

Gomes, F.A.M., Senne, T.A. (2013) A SLP algorithm and its application to topology optimization. Departamento de Matem ́atica Aplicada, IMECC, Universidade Estadual de Campinas, 13083-859, Campinas, SP, Brazil.

Gomes, F.A.M., Senne, T.A. (2013). An SLP algorithm for topology optimization. Retrieve from: http://www.ime.unicamp.br/rel_pesq/2010/pdf/rp07-10.pdf

John H., Beverly H. (1995). Differential equations: a dynamical systems approach. Part ii: higher-dimensional systems. Texts in Applied Mathematics 18. Springer. p. 204. ISBN 978-0-387-94377-0.

Johnsen, S. (2013). Structural Topology Optimization-Basic Theory, Methods and Applications (Master thesis). Academic Archive on Line.

Kosaka, I., Swan, C. C. (1999). A symmetry reduction method for continuum structural topology optimization. Computers and Structures, 70 (1999), 47-61.

Li, Q., Steven, G.P., Osvaldo M., Xie, Y.M. (2000). Structural topology design with multiple thermal criteria. Engineering Computations. Volume 17 issue 6.

Luo, Z., Chen, L. P., Yang, J. Z., Zhang, Y. Q., Karim, A. M. (2004). Fuzzy tolerance multilevel approach for structural topology optimization. Computers and Structures. (2006)127-140.

Matsui, K., Terada, K. (2004). Continuous approximation of material distribution for topology optimization. International Journal for Numerical Methods in Engineering. Volume 59, Issue 14, pages 1925–1944, 14 April 2004.

Michell, A. (1904). The limit of economy of material in frame structures. Philosophical Magazine, 8(6):589–597, 1904.

Mijar, A. R. (1997). Topology design of structures using SLP. (Master thesis). University of Iowa.

Paulino, G. H., Le, C. H. (2009). Research Paper: A modified q4/q4 element for topology optimization. Struct. Multidisc Optim. 37:255–264

Rahmatalla, S. F., Swan, C. C. (2003). Continuum topology optimization of buckling sensitive structure. AIAA Journal vol.41, No.6.

Rahmatalla, S. F., Swan, C. C. (2004). A Q4/Q4 continuum structural topology optimization implementation. Struct. Multidisc Optim. 27:130–135

Rahmatalla, S. F., Swan, C. C. (2003). Form finding of sparse structures with continuum topology optimization. Journal of Structural Engineering – ASCE. 1707—1716.

Rozvany, G. (1976). Optimal design of partially discretized grillages. Journal of the Mechanics and Physics of Solids. Volume 24, Issues 2 – 3, June 1976, Pages 125 – 136.

Sigmund, O., Peterson J. (1998). Numerical Instabilities in Topology Optimization: A Survey on Procedures Dealing With Checkerboards, Mesh-Dependencies And Local Minima. Struct. Multidisc Optim. 16:68–75

Sigmund, O., Torquato, S. (1998). Design of smart composite materials using topology optimization. Smart Mater. Struct.8 (1999) 365–379.

Stainko, R. (2006). Advanced multilevel techniques to topology optimization (Doctoral dissertation). Johannes Kepler University.

Swan, C. C., (2013). Topology optimization with engineering application. Unpublished.

Swan, C. C., Kosaka, I. (1997). Voigt-Reuss topology optimization for structures with nonlinear material behaviors. International Journal for Numerical Methods in Engineering, Vol. 40, 3785-3814

Swan, C. C., Kosaka, I. (1997). Voigt-Reuss topology optimization for structures with linear elastic material behaviors. International Journal for Numerical Methods in Engineering, Vol. 40, 3033-3057.

Swan, C.C., Arora, R.S., Kosaka, I., Mijar, A.R. (1998). Concept design of bridge structures for stiffness and vibrations using continuum topology optimization. In Structural Engineering World Wide, N.K. Srivastava (Ed.), ASCE, Paper T159-4.

V.B. Hammer and N. Olho. (2000). Topology optimization of continuum structures subjected to pressure loading. Struct Multidisc Optim 19, 85-92.

Xu, Z.S., Huang, Q.B., Zhao, Z.G. (2011). Topology optimization of composite material plate with respect to sound radiation. Engineering Analysis with Boundary Elements. Volume 35, Issue 1, January 2011, Pages 61 – 67.

Zhang, W.H. (2003). Dual approach using a variant perimeter constraint and efficient sub-iteration scheme for topology optimization. Computers & Structures Volume 81, Issues 22 – 23, September 2003, Pages 2173 – 2181.